

Accepted Manuscript

Temperature dependence of oxygen- and clumped isotope fractionation in carbonates: a study of travertines and tufas in the 6-95°C temperature range

Sándor Kele, Sebastian F.M. Breitenbach, Enrico Capezzuoli, A. Nele Meckler, Martin Ziegler, Isabel M. Millan, Tobias Kluge, József Deák, Kurt Hanselmann, Cédric M. John, Hao Yan, Zaihua Liu, Stefano M. Bernasconi

PII: S0016-7037(15)00415-9
DOI: <http://dx.doi.org/10.1016/j.gca.2015.06.032>
Reference: GCA 9347

To appear in: *Geochimica et Cosmochimica Acta*

Received Date: 1 December 2014

Accepted Date: 24 June 2015

Please cite this article as: Kele, S., Breitenbach, S.F.M., Capezzuoli, E., Nele Meckler, A., Ziegler, M., Millan, I.M., Kluge, T., Deák, J., Hanselmann, K., John, C.M., Yan, H., Liu, Z., Bernasconi, S.M., Temperature dependence of oxygen- and clumped isotope fractionation in carbonates: a study of travertines and tufas in the 6-95°C temperature range, *Geochimica et Cosmochimica Acta* (2015), doi: <http://dx.doi.org/10.1016/j.gca.2015.06.032>

This is a PDF file of an unedited manuscript that has been accepted for publication. As a service to our customers we are providing this early version of the manuscript. The manuscript will undergo copyediting, typesetting, and review of the resulting proof before it is published in its final form. Please note that during the production process errors may be discovered which could affect the content, and all legal disclaimers that apply to the journal pertain.



1 **Temperature dependence of oxygen- and clumped isotope fractionation in carbonates: a**
 2 **study of travertines and tufas in the 6-95°C temperature range**

3 Sándor Kele^{1,2,*}, Sebastian F.M. Breitenbach³, Enrico Capezzuoli⁴, A. Nele Meckler¹, Martin
 4 Ziegler¹, Isabel M. Millan¹, Tobias Kluge⁵, József Deák⁶, Kurt Hanselmann¹, Cédric M.
 5 John⁵, Hao Yan⁷, Zaihua Liu⁷ and Stefano M. Bernasconi¹

6
 7 ¹Geological Institute, ETH Zürich, Switzerland,

8 ²Institute for Geological and Geochemical Research, Research Centre for Astronomy and Earth Sciences,
 9 Hungarian Academy of Sciences, Budapest, Hungary

10 ³Dept. of Earth Sciences, Univ. of Cambridge, Downing Street, Cambridge CB2 3EQ, UK

11 ⁴Dept. of Phys., Earth and Env. Sci., Univ. of Siena, Italy

12 ⁵Dept. of Earth Sci. and Eng., Qatar Carbonate and Carbon Storage Research Centre, Imperial College, London,
 13 London, Prince Consort Road, London, SW7 2AZ, UK

14 ⁶Gwis Ltd, Dunakeszi, Hungary

15 ⁷State Key Laboratory of Environmental Geochemistry, Institute of Geochemistry, Chinese Academy of
 16 Sciences, Guiyang 550081, China

17 *e-mail: keles@geochem.hu

18
 19 **Abstract**

20
 21 Conventional carbonate-water oxygen isotope thermometry and the more recently developed
 22 clumped isotope thermometer have been widely used for the reconstruction of
 23 paleotemperatures from a variety of carbonate materials. In spite of a large number of studies,
 24 however, there are still large uncertainties in both $\delta^{18}\text{O}$ - and Δ_{47} -based temperature
 25 calibrations. For this reason there is a need to better understand the controls on isotope
 26 fractionation especially on natural carbonates. In this study we analyzed oxygen, carbon and
 27 clumped isotopes of a unique set of modern calcitic and aragonitic travertines, tufa and cave
 28 deposits from natural springs and wells. Together these samples cover a temperature range
 29 from 6 to 95°C. Travertine samples were collected close to the vents of the springs and from
 30 pools, and tufa samples were collected from karstic creeks and a cave. The majority of our
 31 vent and pool travertines and tufa samples show a carbonate-water oxygen isotope
 32 fractionation comparable to the one of Tremaine et al. (2011) with some samples showing
 33 higher fractionations. No significant difference between the calcite-water and aragonite-water
 34 oxygen isotope fractionation could be observed. The Δ_{47} data from the travertines show a
 35 strong relationship with temperature and define the regression $\Delta_{47} = (0.044 \pm 0.005 \times 10^6) / T^2$
 36 $+ (0.205 \pm 0.05047)$. The pH of the parent solution, mineralogy and precipitation rate do not
 37 appear to significantly affect the Δ_{47} -signature of carbonates, compared to the temperature
 38 effect and the analytical error. The tufa samples and three biogenic calcites show an excellent
 39 fit with the travertine calibration, indicating that this regression can be used for other

40 carbonates as well. This work extends the calibration range of the clumped isotope
41 thermometer to travertine and tufa deposits in the temperature range from 6°C to 95°C.

42

43

44 **Keywords:** travertine, tufa, stable and clumped isotopes, calibration, non-equilibrium
45 fractionation

46

47 **1 Introduction**

48

49 Since the early times of stable isotope geochemistry, the oxygen isotope fractionation
50 between calcite and water is one of the most widely used methods to reconstruct the
51 temperature at which calcite has precipitated (McCrea, 1950; Epstein et al., 1953; Kim and
52 O'Neil, 1997; Coplen, 2007). More than 50 years of research have produced a number of
53 theoretical, empirical and laboratory-based calibrations, but significant discrepancies still
54 exist among them. Because laboratory calibrations are challenging, naturally precipitated
55 carbonates are an important source of calibration materials for the oxygen isotope
56 fractionation, provided that temperature and conditions of carbonate precipitation are well
57 known. In this paper we use an extensive set of travertine and tufa samples, precipitated under
58 very different geochemical conditions and in a large but well-constrained temperature range,
59 as a natural laboratory to better understand the dominant controls on the carbonate-water
60 isotope fractionation and on the recently developed carbonate clumped isotope thermometer.

61 Conventional carbonate-water paleothermometry requires knowledge of the oxygen isotope
62 composition of the water from which the carbonate precipitated, which is often impossible to
63 estimate. The carbonate clumped isotope thermometer (Ghosh et al., 2006a) circumvents this
64 problem because it requires no assumptions on the $\delta^{18}\text{O}$ of the precipitating water (Eiler,
65 2007). The theoretical basis of the clumped isotope paleothermometer is the proportionality
66 between observed excess abundance of $^{13}\text{C}^{18}\text{O}$ -bonds in carbonate relative to its stochastic
67 distribution (defined as Δ_{47} , see below) and the carbonate precipitation temperature. This
68 excess abundance of $^{13}\text{C}^{18}\text{O}$ -bonds is independent of the bulk carbonate isotopic composition.

69 Clumped isotope geochemistry has already been applied to a number of materials and
70 questions, for example to soil carbonates (Ghosh et al., 2006b; Snell et al., 2013), speleothems
71 and cryogenic cave carbonates (Affek et al., 2008; Daëron et al., 2011; Kluge et al., 2014a),
72 land snails (Zaarur et al., 2011), brachiopods (Came et al., 2007), and studies on diagenesis
73 and low grade metamorphism (Huntington et al., 2011; Ferry et al., 2011; Budd et al., 2013).

74 One of the open questions hampering a wider use of the carbonate clumped isotope
75 thermometer is the discrepancy between published temperature calibrations (Ghosh et al.,
76 2006a, 2007; Guo et al., 2009; Dennis and Schrag, 2010; Tripathi et al., 2010; Eagle et al.,
77 2010; Thiagarajan et al., 2011; Henkes et al., 2013; Grauel et al., 2013; Zaarur et al., 2013;
78 Tang et al., 2014; Came et al., 2014; Fernandez et al., 2014). The reasons for these differences
79 remain largely unclear. Came et al. (2014) and Fernandez et al. (2014) suggested that the
80 different phosphoric acid reaction temperatures for the conversion of sample carbonate to CO₂
81 may be one of the main causes of discrepancies. However, Defliese et al. (2015) determined
82 the phosphoric acid fractionation factors for mass-47 CO₂ for a range of reaction temperatures
83 for calcite aragonite and dolomite, and suggested that mineralogical and acid fractionation
84 factor differences are not likely the cause of discrepant calibrations. Other differences in the
85 analytical procedures that could alternatively cause discrepancies are the use of common
86 versus individual reaction vessels or the amount of sample and acid used (Wacker et al.,
87 2013). Because with the Kiel IV- MAT 253 system operated at ETH the reaction occurs at
88 70°C and much less sample and acid is used compared to other setups, it is necessary to
89 evaluate the slope resulting from this analytical system.

90 In addition to the discrepancies, most calibrations based on natural samples are limited to
91 temperatures below 45°C. To improve applicability of this method it is vital to extend the
92 range of such calibrations to higher temperatures. Laboratory experiments are challenging,
93 and may not be representative for all naturally occurring carbonates (Henkes et al., 2013),
94 thus, in this study we focused on natural carbonates.

95 Among terrestrial carbonates, clumped isotopes have not yet been applied to travertines, as
96 they are typically considered to be non-equilibrium deposits. Indeed, deviations from the
97 expected oxygen isotope 'equilibrium', as defined from laboratory measurements (Kim and
98 O'Neil, 1997), have been observed in natural carbonates (Gonfiantini et al., 1968; Turi, 1986;
99 Friedman, 1970; Fouke et al., 2000; Coplen, 2007; Kele et al., 2008). However, it is currently
100 unclear which, if any, of the published calibrations represents true equilibrium.

101 The natural calcite from the Devils Hole vein which was analyzed by Coplen (2007), is often
102 argued to be very close to equilibrium due to the very slow growth rates in this subaqueous
103 setting. Travertines are continental carbonates composed mainly of calcium carbonate
104 produced from CO₂ degassing of supersaturated calcium bicarbonate-rich waters, typically
105 hydrothermal in origin. Previous case studies on travertines from Egerszalók (Kele et al.,
106 2008) and Pamukkale and Karahayit (Kele et al., 2011) have shown that travertines
107 precipitating very close to the vent of the springs show oxygen isotope compositions similar

108 to the values predicted by Coplen (2007). Significant deviations are only observed along the
109 flow path with increasing distance from the vents where the water first emerges from the
110 underground. Therefore, we hypothesize that a careful choice of samples collected close to
111 vents offers the possibility to establish a robust clumped isotope calibration to higher
112 temperatures than the range covered by the natural carbonate calibrations published so far.
113 We use calcitic and aragonitic travertines from natural springs and artificial thermal wells
114 covering a temperature range between 5.6 and 95°C. This is a unique sample set, because to
115 date there are no Δ_{47} data available for natural carbonates precipitated at the Earth surface
116 above 50°C. In addition, we analysed also a set of tufa and cave carbonate deposits from
117 karstic waters to evaluate if these deposits would show a similar isotope fractionation. The
118 term tufa refers to continental carbonates typical of karstic areas, composed dominantly of
119 calcite and produced from ambient temperature, calcium bicarbonate-rich waters, containing
120 abundant remains of micro- and macrophytes (Capezzuoli et al., 2014).

121 The main advantages using travertines for the calibration of the clumped isotope thermometer
122 are: 1) Travertines grow over a wide temperature range; 2) the temperature, pH, and
123 chemistry of the depositing water and rate of deposition can be measured in the field; 3) these
124 carbonates represent mainly inorganic deposits and show no biological vital effect; 4) they
125 can form different polymorphs of calcium carbonate (calcite, aragonite).

126 We propose a calibration equation based on vent and open air pool samples only, as they have
127 been shown to be the least likely to be affected by kinetic fractionation effects (Yan et al.,
128 2012; Wang et al., 2014). The carbonate formed close to the vents corresponds to only a small
129 fraction of the total available carbonate dissolved in the water because water rapidly flows
130 away from the vent. For this reason the carbonate closest to the vent orifice records
131 precipitation due to initial degassing of only a small fraction of the CO_2 . This may be the
132 reason why the first precipitates may be closer to the equilibrium conditions corresponding to
133 the temperature of the fluid before its emergence. In the case of the pools the reason may be
134 that there is a very thick water layer, CO_2 degassing is very slow and the precipitation rate is
135 also very low. In this case, H_2O and HCO_3^- are more likely to reach equilibrium. We then
136 evaluate the effects of other factors besides temperature controlling clumped isotope values,
137 such as precipitation rate, CO_2 degassing (change in pH), and evaporation. Finally, we
138 compare the results of these inorganic samples with a set of biogenic carbonates to evaluate if
139 the temperature- Δ_{47} relationship based on travertines is applicable to biogenic samples. Our
140 results will help improve the confidence in paleotemperature reconstructions not only from
141 travertines, but also from cave carbonates, diagenetic cements and biogenic carbonates.

142

143 **2 Description of the sampling sites**

144

145 The sampling sites are presented in Figures 1, 2 and 3. A detailed description for most of the
146 sites is given in Chafetz and Lawrence (1994), Demény et al. (2010) and Yan et al. (2012).
147 Below we describe the newly sampled sites and sampling strategy. The characteristics of all
148 sampled sites are summarized in Table 1.

149

150 **2.1 Travertines**

151 *2.1.1 Central Italian travertines*

152

153 Central Italy is rich in travertine and tufa deposits (Capezzuoli et al., 2011). For this study, we
154 sampled nine of these sites. The thermal spring of Palagio is located in Piacenzian marine
155 clays about 50 km NW of Siena. Thermal water with a pH of 6.57, mean temperature of
156 22.7°C and a discharge of ~1 L/s (Minissale, 2004), forms a small pool with carbonate raft
157 precipitation (Fig. 1A).

158 Bagnoli is located in Piacenzian marine sandy deposits about 20 km NW of Siena. Water
159 chemistry suggests that the water circulates in an anhydrite-dolomite reservoir of Triassic age
160 (Casagli et al., 1990). The Bagnoli water ($T_{\text{mean}} = 23.7^{\circ}\text{C}$, pH = 6.62) presently forms only a
161 thin travertine deposit around the vent but Pleistocene tufa deposits in the area suggest that
162 activity may have been higher in the past (Capezzuoli et al., 2008). Samples were taken at the
163 outlet of a pipe (Fig. 1B).

164 The spring of Acqua Borra is located ~15 km east of Siena in Zanclean marine clays. The
165 thermal water has a mean temperature of 36.1°C, a pH of 6.58 and a low discharge rate,
166 presently issuing from a small pipe (Fig. 1C), where the samples were taken. The water
167 differs from other Tuscan thermal springs for its high salt (>12 g/L, 75% NaCl) and high CO₂
168 content.

169 At Rapolano Terme located ~30 km east of Siena, two springs were sampled. *Terme San*
170 *Giovanni* was the most active travertine-depositing site in the area, until the water was
171 diverted for use in a spa in the 1990s. Calcite raft samples were taken from a small resurgence
172 at the NE termination of a fissure-ridge (Guo and Riding, 1999) (Fig. 1D). The water is rich in
173 calcium, bicarbonate and sulfate, with a pH of 6.53 and $T = 41.2^{\circ}\text{C}$. The second spring,
174 *Madonna al Colle Well*, is an intermittent thermal spring ($T = 28^{\circ}\text{C}$, pH = 6.62) outflowing
175 from a borehole drilled in the 1960s for geothermal exploration. Water flux is controlled by a

176 tap at the top of the borehole, but frequently overflows spontaneously due to fluid
177 overpressure (Fig. 1E). Carbonate encrustations were sampled directly at the well.

178 The Il Doccia spring is characterized by a high temperature ($T = 48.3^{\circ}\text{C}$), relatively low
179 discharge (0.3 L/s; Minissale, 2004) and $\text{pH} = 7.05$. It is located ca. 10 km south of Siena on
180 the Northern Apennines orogenic deposits. Deposition rate is very low, forming a small
181 travertine mound (Fig. 1F).

182 The Bagni di Petriolo area is located 30 km south of Siena. Several active hot springs align
183 along a fault with a mean temperature of 42.5°C and a low-rate discharge of ca. 10 L/s
184 (Minissale, 2004). Travertine and thermal waters ($T = 44.3^{\circ}\text{C}$, $\text{pH} = 6.45$) were taken at the
185 *Bagni di Petriolo* thermal spa (Fig. 1G).

186 The Bagni San Filippo travertine is located on the eastern side of the Middle Pleistocene
187 Monte Amiata volcano (Brogi et al., 2010). Several hot springs emerge at a maximum
188 temperature of 52°C . The *Fosso Bianco* spring ($T = 44.6^{\circ}\text{C}$, $\text{pH} = 6.53$) located along the
189 homonymous creek, in the eastern and lower side of the same-fissured body, was sampled
190 (Fig. 1H).

191 The southern sampled area in the surrounding of Viterbo is located on Middle-to-Late
192 Pleistocene pyroclastics and lavas. The *Piscine Carletti* spring actively precipitates travertine
193 and it is characterized by $T_{\text{mean}} = 57.9^{\circ}\text{C}$, $\text{pH} = 5.67$ and 3.7 L/s discharge (Pentecost, 1995;
194 Di Benedetto et al., 2011) (Fig. 2A).

195

196 2.1.2 Carbonate deposits at Hungarian thermal wells

197

198 Five travertine-depositing sites were sampled in Hungary. At Széchenyi thermal spa
199 (Budapest), groundwater is extracted from a 1257 m deep well from the top of the Triassic
200 aquifer. The sampled carbonate was formed in 2012 in the basement of the spa. Sample Sz.-
201 2/2 was taken directly at a fissure of the tube (Fig. 2B), while water with a temperature of
202 70.9°C and pH of 6.4 was sampled at a tap on the same tube several meters away. The 2092 m
203 deep Tura thermal well was drilled in 1963 as an oil-exploratory borehole and reached thermal
204 karst water discharging with 95°C and $\text{pH} = 6.88$. Deposited travertines cover the whole well-
205 head. The well was closed in 1998, but travertine and water samples were taken in 2000 at a
206 trial-operation of the well after the travertine cover was removed. The travertine sample
207 originates from the earliest deposition after 2000. Carbonate sample Bük-4 was collected
208 from the outflowing water ($T = 54.9^{\circ}\text{C}$, $\text{pH} = 6.88$) of the 1282 m deep Bük-1 thermal well
209 (W Hungary), which supplies the Bük thermal spa with thermal water of 58°C since 1960.

210 The water originates from Miocene porous aquifers. Travertine and water were collected at
211 the standpipe of the well, where excess water is periodically overflowing (Fig. 2C). The spa
212 of Igal is supplied with thermal water ($T = 75^{\circ}\text{C}$, $\text{pH} = 6.89$) of a Triassic and Cretaceous
213 aquifer via the 651 m deep well of Igal 1. Carbonate deposits were sampled from the wall of
214 the tube (Fig. 2D). The Köröm thermal well (NE Hungary) drilled in 1961 hit thermal water
215 (82°C) at 1880 m depth. Travertine and water were sampled directly at the well outlet (sample
216 Kör-13/0, $T = 79.2^{\circ}\text{C}$, $\text{pH} = 6.8$) (Fig. 2E).

217

218 *2.1.3 Baishuitai travertine (China)*

219

220 The Baishuitai travertine, one of the largest travertine deposits in China, is located ~100 km
221 south of Shangri-La Town, Yunnan Province, China (Yan et al., 2012). Two travertine-
222 depositing systems are found here: a fast-flow channel system and slow-flow pool system.
223 The sample P5 ($T_{\text{summer}} = 12^{\circ}\text{C}$, $\text{pH}_{\text{summer}} = 8.14$ and $T_{\text{winter}} = 5.6^{\circ}\text{C}$, $\text{pH}_{\text{winter}} = 8.19$) was taken
224 about 300 m from the vent (spring S1-1) in the pool system (Fig. 2F).

225

226 *2.1.4 Narrow Gauge travertine (Yellowstone)*

227

228 The GeoBio-II spring ($T_{\text{vent}} = 61.1^{\circ}\text{C}$, $\text{pH} = 6.6$) at Narrow Gauge Springs (Mammoth Hot
229 Springs, Yellowstone, USA, Chafetz and Lawrence, 1994) was sampled. Sample NG-2 is a
230 precipitate collected from a rope that was immersed in the water very close to the vent orifice
231 ($T = 60.4^{\circ}\text{C}$, $\text{pH} = 6.6$; Fig. 2G) and represents the precipitation of a few hours.

232

233 *2.1.5 Madre del Agua (Tenerife, Spain)*

234

235 A 20 cm thick calcite encrustation sample and precipitating water were collected at the
236 discharge point of an artificial tunnel at Madre del Agua (Canarian Island) situated in the
237 south-eastern part of Tenerife. Water temperature at the sampling point was 33.8°C , with a
238 pH of 7.7 and a discharge rate 5.3 L/s (Demény et al., 2010).

239

240 *2.2 Tufa and cave tufa samples from Hungary and Italy*

241

242 Tufa samples were collected along a 2.4 km long section in the Szalajka-valley (Szilvásvár,
243 Bükk Mts, Hungary) where supersaturated karstic springs (average runoff is 70 l/sec)

244 precipitate tufa terraces, dams and cascades, further promoting CO₂ degassing and tufa
245 precipitation. Starting from the Szalajka-spring (~8.6°C) three samples (Szal-2, Szal-6, Szal-
246 15; Fig. 3A,B,C; Table 1) were sampled in October along the flow path downstream 413 m (T
247 = 10.1°C, pH = 8.45), 773 m (T = 11°C, pH = 8.55) and 2462 m (T = 12.1°C, pH = 8.53)
248 from the spring, respectively.

249 Three tufa samples with temperatures ranging from 11°C to 20.7°C were collected from
250 Sarteano, Rapolano Terme (Canatoppa Creek) and La Pigna (all in Tuscany, Italy). The
251 Sarteano tufa is located along the Fosso dei Mulini Creek in Sarteano village. Water
252 originates from a private pool about 100 m upstream from the sampling point (T = 20.7°C, pH
253 = 8.92) and the entire creek is carbonate-encrusted (Fig. 3D). The Canatoppa tufa (Rapolano
254 Terme) precipitate along the Canatoppa Creek (Fig. 3E) from water with a temperature of
255 11°C and pH of 8.94, north of the travertine fissure ridge at the Terme San Giovanni
256 described above. The La Pigna tufa is a perched spring tufa deposit formed from a small
257 resurgence south of Siena. We sampled the frontal portion of the system, about 20 m from the
258 spring point and below a 4 m-high cascade, where the temperature of the water is 12.5°C and
259 the pH is 8.61 (Fig. 3F). In order to represent different depositional environments, a recent
260 cave tufa (flowstone) sample precipitated from flowing water was additionally taken from the
261 Havasok tufa (Baradla cave, Aggtelek Karst, Hungary). The Havasok tufa dam (Fig. 3G)
262 forms from a thin, periodically flowing water film (~9.5°C).

263

264 **3 Methods**

265

266 *3.1 Sampling and in situ analyses*

267

268 In all cases only the uppermost surface of the recent travertine was sampled to ensure the
269 collection of freshly precipitated carbonates. Water samples were collected in 100 ml glass
270 bottles for stable oxygen isotope analyses. In situ measurements of temperature, pH and
271 electric conductivity (EC) of water were conducted at all sampling points using various
272 instruments: 1) At the Italian sites a Hanna HI 98130 meter was employed (precision: T =
273 ±0.1°C, pH = ±0.01). 2) The Yellowstone site was probed with a Hach HQ40d meter
274 (precision: T = ±0.1°C, pH = ±0.1). 3) At the Szalajka Creek a VWR EcoSense pH10
275 pH/Temperature Pen (precision: T = ±0.3°C, pH = ±0.02) was used, while conductivity was
276 measured with a Eutech Digital pH/EC Pen. 4) The Hungarian thermal wells were probed

277 with a WTW Multi 1970i meter with automatic temperature compensation to 20°C (precision:
278 $T = \pm 0.1^\circ\text{C}$, $\text{pH} = \pm 0.01$).

279 At some sites the deposition rate could be calculated using the weight of carbonate deposited
280 on plexiglass substrates. The amount of modern travertine deposited on the plexiglass
281 substrates was determined by measuring the weight increase of the substrates. The detailed
282 description of the calculation can be found in Liu et al. (2010) and in Yan et al. (2012). In
283 cases where the placement of substrates was not possible the deposition rate (log R) was
284 estimated based on the size of the carbonate deposit. An annual change of the local carbonate
285 depositional morphology imply an intensive-to-moderate precipitation rate (cm/year), while a
286 slightly modified morphology implies a moderate-to-low precipitation rate (mm/year).
287 Considering the high deposition rates, the ages of sampled carbonates are estimated to be at
288 maximum several days for travertines or a few months for tufa.

289

290 *3.2 X-ray diffraction, electron microprobe, and stable isotope analyses*

291

292 The mineralogy of all carbonate samples was determined by X-ray powder diffraction (XRD)
293 using a Philips PW 1710 diffractometer (with $\text{CuK}\alpha$ radiation at 45 kV and 35 mA) at the
294 Institute for Geological and Geochemical Research, Hungarian Academy of Sciences (IGGR-
295 HAS, Budapest). Semi-quantitative phase analysis was made on randomly oriented samples
296 using the peak area of calcite 104 and aragonite 111 reflections (Bárdossy et al., 1980). The
297 relative error of the quantification is 5–10%. The mineralogy of some samples has been
298 determined at ETH Zürich using a Bruker AXS D8 Advance instrument. In order to determine
299 the size of individual crystals from the travertine deposits, electron microprobe analyses were
300 carried out at IGGR-HAS using a JEOL JXA-733 instrument.

301 All carbonate samples were powdered and homogenized using an agate mortar and pestle.
302 Carbon and oxygen isotope analyses of bulk carbonate samples were carried out as part of the
303 clumped isotope analyses with a Thermo Fisher Scientific Kiel IV preparation device coupled
304 to a Thermo Fisher Scientific MAT 253 isotope ratio mass spectrometer. For oxygen and
305 carbon isotopes the performance of the instrument was monitored with the 4 internal
306 standards ETH-1 ($\delta^{13}\text{C} = 2.14\text{‰}$, $\delta^{18}\text{O} = -1.87\text{‰}$), ETH-2 ($\delta^{13}\text{C} = -10.11\text{‰}$, $\delta^{18}\text{O} =$
307 -18.76‰), ETH-3 ($\delta^{13}\text{C} = 1.81\text{‰}$, $\delta^{18}\text{O} = -1.77\text{‰}$) and ETH-4 ($\delta^{13}\text{C} = -10.10\text{‰}$, $\delta^{18}\text{O} =$
308 -18.76‰), which are measured daily to carry out the corrections for clumped isotopes (see
309 below). The composition of these internal standards was determined using NBS 19 ($\delta^{13}\text{C} =$
310 1.95‰ and $\delta^{18}\text{O} = -2.2\text{‰}$) and NBS 18 ($\delta^{13}\text{C} = 5.05\text{‰}$ and $\delta^{18}\text{O} = -23.1\text{‰}$). The reference

311 gas used in the mass spectrometer is a commercial compressed gas tank, purity 99.99 % with
 312 a $\delta^{13}\text{C}_{\text{VPDB}}$ value of -7.25‰ and a $\delta^{18}\text{O}_{\text{VPDB}}$ value of $+1.65\text{‰}$. $\delta^{18}\text{O}$ analyses of waters were
 313 carried out at IGGR-HAS with a Thermo Fisher Scientific Delta Plus XP mass spectrometer
 314 using the CO_2 -water equilibration method (Epstein and Mayeda, 1953). In case of the water
 315 samples, the in-house laboratory standards BWS-1, BWS-2 and BWS-3 were used, which are
 316 calibrated against Vienna Standard Mean Ocean Water (V-SMOW) with International
 317 Certification (SMOW, GISP and SLAP). Standard BWS-1 ($\delta^{18}\text{O} = -0.60 \pm 0.1\text{‰}$) was made
 318 from seawater and locally sampled lake water; BWS-2 ($\delta^{18}\text{O} = -10.50 \pm 0.1\text{‰}$) was prepared
 319 from tap water; and BWS-3 ($\delta^{18}\text{O} = -20.00 \pm 0.1\text{‰}$) was made from snow from the Tatra
 320 Mountains and Budapest (Kármán et al., 2014). Isotopic compositions are expressed in the
 321 conventional δ notation in ‰ relative to V-PDB for carbonates and V-SMOW for water.
 322 Reproducibility was better than $\pm 0.1\text{‰}$ for carbonate $\delta^{13}\text{C}$ and $\delta^{18}\text{O}$ and better than $\pm 0.2\text{‰}$ for
 323 $\delta^{18}\text{O}$ of waters. The fractionation between carbonate and water are calculated from measured
 324 $\delta^{18}\text{O}_{\text{carbonate}}$ and $\delta^{18}\text{O}_{\text{water}}$, where the fractionation factor is defined as $\alpha = (1 + \delta^{18}\text{O}_{\text{calcite}}/1000)$
 325 $/ (1 + \delta^{18}\text{O}_{\text{water}}/1000)$. $\delta^{18}\text{O}$ values of the three aragonitic travertines (Köröm, Széchenyi
 326 thermal spa, Palagio) were corrected by -0.42‰ , to account for the different phosphoric acid
 327 digestion fractionation factor for aragonite (Kim et al., 2007).

328

329 *3.3 Clumped isotope analyses*

330

331 Carbonate isotopologue measurements were performed using a Thermo Fisher Kiel IV
 332 preparation device coupled to a Thermo Fisher MAT 253 isotope ratio mass spectrometer as
 333 described by Schmid and Bernasconi (2010), modified to include a Porapak trap eliminating
 334 contaminants. The full procedure, including a new correction scheme, has been described by
 335 Meckler et al. (2014). Briefly, per run 8-10 aliquots of 150-220 μg of two samples were
 336 prepared and analysed in microvolume mode together with 8-10 aliquots each of 2 internal
 337 carbonate standards. The $\delta^{13}\text{C}$, $\delta^{18}\text{O}$ and clumped isotope composition is calculated as the
 338 average of the 8 to 10 analyses. Each analysis consisted of 6 cycles of 26 sec integration and
 339 10 sec idle time after changeover valve switch. Initial m/z 44 beam intensities averaged
 340 around 23 V, decreasing to around 13 V after 7 cycles. The temperature-dependent mass 47
 341 anomaly is defined as (Ghosh et al., 2006a):

$$342 \quad \Delta_{47}(\text{‰}) = \left[\left(\frac{R^{47}}{R^{47*}} - 1 \right) - \left(\frac{R^{46}}{R^{46*}} - 1 \right) - \left(\frac{R^{45}}{R^{45*}} - 1 \right) \right] \times 1000 ,$$

343 where R^i is the abundance of the minor isotopologues relative to the most abundant
344 isotopologue with mass 44, and the expected stochastic ratios R^{i*} are calculated based on the
345 measured abundance of ^{13}C and ^{18}O in the sample.

346 The results for standards and samples were corrected offline for pressure baseline (PBL)
347 effects (Bernasconi et al., 2013, Meckler et al., 2014) and were transferred to the absolute
348 reference frame (Dennis et al., 2011) by means of an empirical transfer function (ETF) based
349 on heated and equilibrated gases measured during an earlier period (Meckler et al., 2014).
350 Afterwards, an acid fractionation correction of +0.064‰ was applied to the Δ_{47} , which results
351 from a linear scaling of the observed offset between 25°C and 90°C acid temperature (Henkes
352 et al., 2013) to our reaction temperature of 70°C. Subsequent correction steps for sample
353 results were based on carbonate standards only: The results were first corrected for offsets
354 between measured and accepted values of four in-house carbonate standards, averaged within
355 a moving window encompassing 11 standards (~5 days of measurements). Finally, small
356 differences in scale compression during the measurement periods compared to the initial ETF
357 period were monitored and corrected for with a transfer function based again on the four
358 standards, which strongly differ in bulk isotopic composition and ordering state. The
359 “accepted” Δ_{47} of the standards used for these corrections are (in parenthesis the sample
360 names used in Meckler et al. 2014): ETH-1 (ISO A) = 0.267‰, ETH-2 (ISO B) = 0.269‰;
361 ETH-3 (ISO R) = 0.524‰ and ETH-4 (ISO C) = 0.705‰. Our internal Carrara marble (MS2)
362 standard has a Δ_{47} value of 0.397‰ and NBS 19 yielded a Δ_{47} value of 0.390‰ \pm 0.005 (n =
363 3). Both these values are well in the range of published values for Carrara marbles and NBS
364 19 (Dennis et al., 2011). The four ETH carbonate samples are available as 1g aliquots upon
365 request from S. Bernasconi.

366 Each sample was measured at least three times on different days (with 8-10 aliquots
367 each). The reported results are the averages of the three or more measurements, and reported
368 errors are standard errors of these averages. The long-term reproducibility of the method
369 based on standards is ± 0.012 – 0.016 ‰ (1 SD) (Meckler et al., 2014). The confidence intervals
370 of the regressions were calculated according to Sachs (1984).

371

372 **4 Results**

373

374 *4.1 Physico-chemical parameters, deposition rate and isotopic composition of thermal and*
375 *karstic waters*

376

377 The physico-chemical parameters of the spring waters are summarized in Table 1. For
378 travertines, temperatures ranged from 5.6°C to 95°C, pH ranged from 5.7 to 8.2, and
379 Electrical Conductivity (EC) varied from 1.38 to >20 mS cm⁻¹. $\delta^{18}\text{O}_{\text{water}}$ values ranged from
380 -17.9‰ to -4‰. Where deposition rates could be measured, they ranged from 0.05 and 28.5
381 mg cm⁻²d⁻¹ at the Italian Sites, and were determined as 0.44–2.5 mg cm⁻²d⁻¹ at Baishuitai (Yan
382 et al., 2012).

383 The three tufa samples from Italy were precipitated from waters of 11–20.7°C; the pH varied
384 between 8.61–8.94, while EC values ranged from 0.55 to 2.11 mS/cm. Karstic water samples
385 from the Szalajka Creek showed temperatures between 10.1 and 12.1°C, pH between 8.45 and
386 8.55, EC between 0.473 and 0.503, and $\delta^{18}\text{O}_{\text{water}}$ values from -10.7 to -10.6‰.

387 The values reported here correspond to individual measurements at time of the sampling.
388 However, because the travertine depositing waters are old and derive from deep geothermal
389 circulation systems, their $\delta^{18}\text{O}$ values and physico-chemical parameters do not show seasonal
390 variations. In case of tufa sites minor seasonal changes might occur in both temperature and
391 $\delta^{18}\text{O}_{\text{water}}$, as these are more influenced by rainfall and seasonal change of ambient temperature
392 and insolation and they form further downstream, as in general there is no carbonate
393 deposition in the spring's orifice. However, due to the facts that sampling has been performed
394 mainly during dry season and that carbonate deposition is rapid (up to a few months for the
395 tufa samples), we can assume that the temperatures, measured during sampling campaigns,
396 adequately represent the growth temperatures of the samples.

397

398 *4.2 Mineralogy*

399

400 All samples are mainly composed of calcite, aragonite or their mixture (Table 1). Samples
401 containing elemental sulfur (Il Doccio, Bagni di Petriolo, Table 1) were excluded from
402 clumped isotope analysis as sulfur can affect the clumped isotope signal. Based on SEM
403 analyses, individual crystal size varies not only between samples but also within samples and
404 according to mineral phase. Travertine samples are composed mainly of complex calcite
405 crystals (~10–100 μm), with some exhibiting a dendritic morphology. Aragonite (~100 μm)
406 and gypsum crystals (100–150 μm) are also present in some samples (Fig. 4).

407

408 *4.3 Stable isotopic composition of travertine and tufa samples*

409

410 Carbon and oxygen isotope compositions of all travertine and tufa samples are reported in
411 Table 1. $\delta^{13}\text{C}$ and $\delta^{18}\text{O}$ values range between -11.27‰ and $+7.45\text{‰}$ and between -24.51‰
412 and -5.43‰ , respectively. Tufa collected downstream from the karstic water of the Szalajka
413 Creek show a small increase in $\delta^{13}\text{C}_{\text{tufa}}$ (from -10.2‰ to -9.43‰) and decrease in $\delta^{18}\text{O}_{\text{tufa}}$
414 (from -8.47‰ to -9.30‰) (Table 1). The Havasok cave tufa shows similar $\delta^{13}\text{C}$ (-10.95‰)
415 and a bit higher $\delta^{18}\text{O}$ (-7.73‰) values compared to the Szalajka tufa samples taken from the
416 surface (Table 1). $\delta^{13}\text{C}$ values of the Italian tufa sites are similarly low (between -11.27‰
417 and 0.55‰) and $\delta^{18}\text{O}_{\text{tufa}}$ values vary from -7.39‰ to -5.66‰ . In Figure 5A we plotted the
418 carbonate–water $1000\ln\alpha$ values against temperature. The regression through the travertines
419 alone (diamonds and squares) shows a steeper slope than commonly observed in carbonates
420 (e.g. Kim and O’Neil, 1997; Tremaine et al., 2011). A regression through the entire dataset
421 including the tufa and cave carbonates (Triangles), however, defines a slope and intercept
422 much closer to the one of Tremaine et al. (2011) (see discussion below). No significant
423 difference is observed between aragonite and calcite samples (Fig. 5B).

424

425 4.4 Δ_{47} values of travertine, tufa, and biogenic samples

426

427 Δ_{47} values of travertine and tufa samples vary between $0.510\pm 0.012\text{‰}$ and $0.760\pm 0.008\text{‰}$
428 (Table 1). The three downstream tufa samples from the Szalajka Creek show no systematic
429 trend and Δ_{47} values are between $0.732\pm 0.008\text{‰}$ and $0.760\pm 0.008\text{‰}$ (Table 1). The Havasok
430 cave tufa shows a very similar Δ_{47} value ($0.756\pm 0.01\text{‰}$). The Sarteano, Canatoppa and La
431 Pigna tufa samples yielded Δ_{47} values between $0.703\pm 0.009\text{‰}$ and $0.742\pm 0.008\text{‰}$ (Table 1).
432 When plotted against temperature (Fig. 6A, B), all samples show a very good fit in spite of
433 the different depositional environments. In addition, we did not observe a systematic
434 difference between calcite and aragonite samples (Fig. 6B). For comparison we also analyzed
435 three biogenic carbonates, which were previously analyzed for Δ_{47} and described in detail by
436 Wacker et al. (2014) (Table 2). All three samples fit very well on the regression defined by
437 the travertines. The Δ_{47} value of $0.648\pm 0.014\text{‰}$ of the ostrich eggshell compares very well
438 with the $0.643\pm 0.005\text{‰}$ obtained by Wacker et al. (2014). For *D. wyvillei* we obtained a Δ_{47}
439 value of $0.742\pm 0.009\text{‰}$, which is 0.29 higher than the $0.713\pm 0.009\text{‰}$ reported by Wacker et
440 al. (2014) and for *A. Islandica* we obtain a value of $0.759\pm 0.004\text{‰}$, 0.035 higher than the
441 value reported in Wacker et al. (2014).

442

443 5 Discussion

444

445 *5.1 Oxygen isotope fractionation*

446

447 The temperature dependence of the oxygen isotope fractionation in our samples is compared
448 with that of other studies in Figure 7. The majority of our vent and pool travertines show a
449 higher mineral-water oxygen isotope fractionation than the Kim and O'Neil (1997) study, in
450 agreement with the results of Kele et al. (2008, 2011), and many of them fit well on the
451 curves published by Coplen (2007), Tremaine et al. (2011) and Affek and Zaarur (2014). Our
452 travertine data alone define a fractionation that can be expressed as $1000\ln\alpha = (20\pm 2) \times$
453 $1000/T - (36\pm 7)$ ($R^2 = 0.96$). This slope is steeper than the previously published curves and is
454 strongly influenced by 5 samples with very high fractionation. The cause of these very high
455 fractionations is not clear, and we could find no relationship with any physico-chemical
456 parameter we have measured, but similar high fractionations have also been reported by Kele
457 et al. (2011) in other travertines and seem to be a common feature that needs additional
458 studies. Possible causes for changes in isotope fractionation are pH variations (e.g. Zeebe,
459 1999), but we do not observe a systematic positive offsets with decreasing pH as it would be
460 expected if pH were a major controlling factor. A more comprehensive discussion of the
461 oxygen isotope fractionation based on a much larger dataset will be published elsewhere.

462 In case of the Szalajka spring section the $\delta^{18}\text{O}_{\text{carbonate}}$ show slight downstream increase (from
463 -10.2 to -9.44 ‰), while the $\delta^{18}\text{O}_{\text{water}}$ is nearly constant (-10.6 ‰) (Table 1). The water
464 temperature of the Szalajka Creek increases slightly downstream (from 10.1°C to 12.1°C ,
465 Table 1) due to radiation and contact with the atmosphere, which is warmer than the cold
466 karstic water. This downstream temperature increase can cause the decreasing $\delta^{18}\text{O}_{\text{carbonate}}$
467 values along the flow path. If we include the tufa samples deposited from cold karstic waters,
468 the regression line becomes $1000\ln\alpha = (16.8\pm 1.7) \times 1000/T - (26\pm 5.4)$ ($R^2 = 0.95$) (Fig. 5A),
469 which is indistinguishable from the regression line of Tremaine et al. (2011) and the results of
470 the surface precipitation experiments of Affek and Zaarur (2014), confirming that these
471 regression lines are valid to temperatures of up to 95°C . In spite of the fact that travertines
472 have generally very high precipitation rates (see below), which could lead to lower apparent
473 oxygen isotope fractionation, no significant difference between the calcite-water and
474 aragonite-water oxygen isotope fractionation is observed (Fig. 5B).

475

476 *5.2 Temperature dependence of Δ_{47} in travertines and tufa*

477

478 Figures 6A and 6B show the T- Δ_{47} relationship for the entire sample set defining an excellent
 479 correlation of Δ_{47} with the temperature of deposition. If we only use the travertine samples
 480 collected at temperatures between 5.6 and 95°C and exclude the tufa to avoid mixing of two
 481 groups of samples that potentially have different characteristics to define the T- Δ_{47}
 482 relationship, we obtain:

$$484 \quad \Delta_{47} = (0.044 \pm 0.005 \times 10^6) / T^2 + (0.205 \pm 0.047) \quad R^2 = 0.96 \quad (\text{eq. 1})$$

485
 486 The tufa samples and the three biogenic samples fit well within the error of the regression,
 487 supporting the validity of the travertine calibration also for tufa formed in karstic
 488 environments.

489 The Δ_{47} value of the calcite raft sample collected from the Terme San Giovanni fissure ridge
 490 (Table 1, Fig. 6B) shows a positive offset compared to the empirical calibration line. If this
 491 outlier is discarded from the calibration data set, the r^2 increases to 0.99, while *eq. 1* does not
 492 change significantly. This positive offset cannot be explained by enhanced disequilibrium at
 493 the surface of the solution (Affek and Zaarur, 2014), as this would produce Δ_{47} values below
 494 the calibration line. For this sample, the water temperature was measured below the water
 495 surface, while the raft sample could record slightly lower water temperature at the water-air
 496 interface, potentially explaining a small part of the 10°C offset. Affek et al. (2014) similarly
 497 found enriched Δ_{47} in a surface raft sample from a cave pool and speculated that the reason
 498 could be reduced super-saturation of the precipitating water compared to other speleothem
 499 formation sites due to prior calcite precipitation.

500 For the karstic Szalajka Creek, tufa deposition only starts 400 m further downstream of the
 501 spring. Δ_{47} values of tufa deposits collected downstream show no systematic trend with
 502 distance from the discharge point and the samples scatter around the travertine regression
 503 (Fig. 6A). The lack of any systematic downstream effect on Δ_{47} may be explained by the
 504 relatively constant water temperatures along the stream and relatively low precipitation rates.
 505 This shows that there is no significant influence of kinetic fractionation effects on Δ_{47} in these
 506 tufa samples. It is also noteworthy that the three biogenic samples analyzed fit very well on
 507 the calibration line (Fig. 6A), indicating that this calibration is potentially useful also for
 508 biogenic materials.

509 Comparison with other published T- Δ_{47} calibrations (Fig. 8) shows that the slope of our
 510 regression line is intermediate between a group of steeper ones, derived from 25°C acid
 511 digestions (Ghosh et al., 2006a; Tripathi et al., 2010; Zaarur et al., 2013; Came et al., 2014)

512 and a group of shallower slopes, produced with 90°C acid digestions (Dennis and Schrag,
513 2010; Henkes et al., 2013; Eagle et al., 2013; Wacker et al., 2014; Kluge et al., 2015). The
514 difference between our calibration and the one of Wacker et al. (2014) is due to the higher
515 values we obtain for the samples grown at cold temperatures, whereas for the Ostrich eggshell
516 formed at 38°C we obtained the same Δ_{47} value. This could be seen as further evidence for the
517 supposed relationship between calibration slopes and carbonate acid digestion temperature of
518 carbonates (Fernandez et al., 2014), with a stronger influence on samples with high Δ_{47} values.
519 However, this explanation has recently been questioned by the experiments of Defliese et al.
520 (2015). It must furthermore be noted that other effects can influence the slope of the T- Δ_{47}
521 relationship, exemplified by two recent studies reporting shallow slopes, despite acid
522 digestions at 25°C: The surface precipitate calibration of Affek and Zaarur (2014) and the
523 recent calibration of Petrizzo et al. (2014). In view of these unknowns, it is important to
524 increase the efforts to understand the origin of these differences including interlaboratory
525 calibration exercises and studies of other possible causes for discrepancies such as the sample
526 to acid ratio and/or factors influencing the re-equilibration of CO₂ with water during the
527 digestion (Defliese et al., 2015). Considering the systematic differences in the slopes of the
528 calibrations obtained with different analytical setups it is important that the calibration used to
529 calculate temperatures was produced with a similar system as used for the samples. One
530 advantage of the high-temperature digestions at 70 and 90°C is the increased reaction rate that
531 improves the sample throughput and allows an automatisisation of the extraction system (e.g.
532 Passey et al., 2010; Meckler et al., 2014) which is not possible for reactions at 25°C.

533

534 *5.3. Effects of depositional environment on the Δ_{47} values: places of equilibrium and*
535 *disequilibrium*

536

537 The data presented in this study are derived from samples that were carefully chosen to
538 minimize kinetic fractionation effects. We chose only vent and pool samples, which have
539 been shown to be least affected by kinetic fractionation due to progressive degassing (Yan et
540 al., 2012; Wang et al., 2014). The $1000\ln\alpha$ values for most of the samples in this study are
541 close to the original regression line of Kele et al. (2011) and the one of Tremaine et al. (2011),
542 but some samples show higher $\delta^{18}\text{O}$ values. As already noted by Affek and Zaarur (2014),
543 rapid degassing may induce additional fractionation in $\delta^{18}\text{O}$, leading to higher carbonate $\delta^{18}\text{O}$.
544 We observe here an even larger extent of fractionation in carbonate $\delta^{18}\text{O}$ than what has been
545 observed by Affek and Zaarur (2014). At present it is unclear what the cause of this

546 divergence is, but our data confirms the observations of Affek and Zaarur (2014) that these
547 higher fractionations in $\delta^{18}\text{O}$ do not seem to be reflected in the clumped isotope data.

548 The depositional environments for the different samples in this study are very diverse. Where
549 CO_2 degassing rate is fast and the dissolved carbonate and calcium contents of the water are
550 high enough, travertine deposition starts directly at the spring orifice (e.g. Fig. 2D).
551 Sometimes, however, deposition begins only further downstream: e.g., at Pamukkale,
552 carbonate precipitation only starts 155 m downstream from the spring (Kele et al., 2011). If
553 the spring discharges inside a pool, deposition can take place on the surface of the pool in
554 form of calcite rafts (Fig. 1A). Deposition can also occur at the bottom or at the pool rim.
555 Although the mechanism and rate of precipitation in the pools is different from vents (much
556 lower precipitation rate in the pools), Δ_{47} data of pool travertine agree well with the vent
557 travertine calibration curve (Fig. 1A). In pools, with slow carbonate deposition, oxygen
558 isotope exchange between dissolved bicarbonate and H_2O drives oxygen and clumped isotope
559 values towards equilibrium. In cases of limited degassing and very slow carbonate
560 precipitation, the DIC can approach full oxygen isotope exchange with water, leading to
561 equilibrium $\delta^{18}\text{O}$ and Δ_{47} values (Affek et al., 2008). At artificial wells, the chosen deposits
562 are mainly carbonate encrustations on tubes (e.g. Rapolano Terme, Fig. 1E) and these fit the
563 vent and pool data very well.

564 Disequilibrium growth conditions can cause significant changes in both $\delta^{18}\text{O}$ and Δ_{47} . Kinetic
565 isotope effects during rapid CO_2 degassing can lead to higher $\delta^{18}\text{O}$ (and $\delta^{13}\text{C}$), but lower Δ_{47}
566 values (Guo et al., 2008; Affek, 2013). This inverse correlation was observed in modern
567 speleothems (Daëron et al., 2011; Wainer et al., 2011; Kluge and Affek, 2012; Kluge et al.,
568 2013), which are potentially more susceptible to kinetic isotope effects than carbonates
569 precipitated in bulk solution (Affek et al., 2008). Theoretical calculations of Guo (2008)
570 indicated that for each 1‰ increase in $\delta^{18}\text{O}$ a reduction of 0.0175-0.029‰ in Δ_{47} should
571 occur. Guo (2008) explained the kinetic effects as a consequence of irreversible dehydration
572 or dehydroxylation of carbonic acid or bicarbonate (respectively), followed by outgassing of
573 dissolved CO_2 . In Figure 9B we cross-plot the deviation of $1000\ln\alpha$ and Δ_{47} from the
574 respective regression curves to evaluate if positive offsets in $\delta^{18}\text{O}$ are systematically
575 correlated with negative offsets in Δ_{47} . We point out that calculating the deviation from the
576 regression line does not necessarily imply that the observed correlation represents isotopic
577 equilibrium. However the excellent correlation with temperature strongly suggests that
578 temperature is the dominant control on both Δ_{47} and $\delta^{18}\text{O}$ in our dataset. No correlation is
579 observed if the deviation in $1000\ln\alpha$ is calculated with respect to the published curves of Kim

580 and O'Neil (1997) and Tremaine et al. (2011). The lack of correlation suggests that no
581 significant kinetic isotope effect related to degassing in our sample set. The average Δ_{47} offset
582 (0.009‰, $\approx 3.7^\circ\text{C}$) is lower than the standard error of the Δ_{47} values (0.011‰ on average;
583 Table 1, Fig. 9B), and the average $1000\ln\alpha$ offset of travertines is 0.647‰ ($\approx 3.5^\circ\text{C}$).
584 The mean Δ_{47} value of the slowly precipitating subaqueous Devils Hole vein calcite, which
585 has been assumed to grow under isotopic equilibrium conditions (Coplen, 2007; Kluge et al.,
586 2014b), locates slightly above (but within the confidence limits of) the empirical travertine
587 curve (Fig. 6A). This offset is in line with initial results from a laboratory inter-comparison
588 study using the four carbonate standards that suggest that Δ_{47} results at Yale University tend
589 to be higher than at ETH (by 0.007 - 0.045‰; average = 0.025 ‰). Considering the current
590 uncertainties in interlaboratory data comparability, these data suggest that vent and pool
591 travertines, which are the least likely to be affected by kinetic fractionation based on previous
592 stable isotope studies (Kele et al., 2008; Kele et al., 2011; Yan et al., 2012; Wang et al.,
593 2014), in relation to their clumped isotope composition probably represent close to
594 equilibrium precipitation in the entire 5.6-95°C temperature range.

595

596 *5.4 Effect of mineralogy (calcite-aragonite) on the Δ_{47} values*

597

598 Travertine and tufa are mostly composed of inorganic calcite and aragonite and can be used to
599 assess the effect of CaCO_3 polymorphism. Theoretical models of Schauble et al. (2006)
600 suggested that the calcite and aragonite crystal structure and cation substitution (Mg vs. Ca)
601 should have a modest influence of the abundance of ^{13}C - ^{18}O bonds, and theoretical
602 calculations of Guo et al. (2009) similarly predicted different Δ_{47} -T calibration lines for
603 calcite and aragonite for the 260-1500 (K) temperature range. The predicted difference in Δ_{47}
604 between aragonite and calcite is between 0.017‰ (278 K) and 0.0095‰ (363 K) for the
605 temperature range covered in our study. Our sample set contains pure calcitic, almost pure
606 aragonitic and mixed calcitic-aragonitic samples (Table 1). The aragonite-rich samples from
607 Palagio (22.7°C, 99% aragonite) and the other samples with aragonite contents above 80%
608 which were precipitated at temperatures $>56^\circ\text{C}$, all fit within analytical error onto the
609 regression line from all samples (Fig. 6B). A mixed sample with low (<35%) aragonite
610 content (Rapolano Terme, T=28°C) is also on the calibration line. Therefore, our results
611 suggest that aragonite and calcite exhibit a very similar Δ_{47} -T relationship. Similarly, many
612 other studies on biogenic and synthetic carbonates did not resolve any clear mineralogical

613 effects (Tripathi et al., 2010; Thiagarajan et al., 2011; Zaarur et al., 2013; Henkes et al., 2013;
614 Defliese et al., 2015; Kluge and John, 2015).

615

616 *5.5 Effect of pH*

617

618 pH can have an important effect on the oxygen isotopic composition of CaCO_3 since it
619 controls the dissolved carbonate species in the travertine precipitating water, hence the $\delta^{18}\text{O}$
620 and Δ_{47} of the mineral (Usdowski et al., 1991; Zeebe 1999, 2007; Beck et al., 2005; Dietzel et
621 al., 2009; Hill et al., 2014). The dominant DIC species at low pH (<6) is CO_2 (aq), at
622 intermediate pH (6-9.5) HCO_3^- , while at high pH (>10.5) CO_3^{2-} becomes dominant. The $\delta^{18}\text{O}$
623 and the Δ_{47} of the DIC species decrease in this sequence (Zeebe, 1999; Hill et al., 2014).
624 Therefore, carbonates precipitated at higher pH may result in lower $\delta^{18}\text{O}$ and lower Δ_{47} values
625 due to higher proportion of CO_3^{2-} in the DIC (McCrea, 1950; Usdowski et al., 1991; Hill et
626 al., 2014). Based on theoretical calculations of Guo (2008) CO_3^{2-} is estimated to be $\sim 0.018\%$
627 lower in Δ_{47} than HCO_3^- , while the $\delta^{18}\text{O}$ value of the CO_3^{2-} is $\sim 7\%$ lower at 25°C (Beck et al.,
628 2005; Kim et al., 2006).

629 It is somewhat difficult to assess the effect of pH on our sample set, because changes in pH
630 cannot be isolated from other parameters such as T, degassing rate, and ionic strength. The pH
631 for the travertines varies between 5.6 and 7.7, which is lower than the pH typically used for
632 laboratory-based calibrations (Ghosh et al., 2006a; Zaarur et al., 2013), and two travertine
633 pool samples were precipitated at a pH of 8.1. In Figure 10 we grouped the samples by pH,
634 and the lack of systematic offsets suggests that pH has no major influence on Δ_{47} in our
635 sample set. The experimental study of Tang et al. (2014) ($8.3 \leq \text{pH} \leq 10.5$ at 5°C , 25°C and
636 40°C) concluded that there are no clear effects of variable pH, ionic strength and growth rate
637 on the measured Δ_{47} values.

638

639 *5.6 Effect of precipitation rate*

640

641 Recent studies by Dietzel et al. (2009), Day and Henderson (2010) and Gabitov et al. (2012)
642 emphasized the fact that oxygen isotope fractionation between calcite and water can be
643 affected by the precipitation rate of calcite. Their experiments showed that high carbonate
644 precipitation rates drive $\delta^{18}\text{O}_{\text{carbonate}}$ to lower values. Deposition rate might affect the Δ_{47}
645 values, too. Saenger et al. (2012) studied rapidly calcifying hermatypic corals and suggested
646 that their higher than expected Δ_{47} values might be caused by fast calcification, while slowly

647 calcifying corals are close to or within the range of data from inorganic experiments (Ghosh
648 et al., 2006a). Based on theoretical calculations and precipitation experiments, Tripathi and Hill
649 (2014) suggested that the crystal may inherit the Δ_{47} value of the DIC species and thus record
650 a disequilibrium mineral composition, when the growth rate is high, while DIC speciation
651 effects are likely to be negligible for slow-growing crystals.

652 In case of the studied travertines the precipitation rate (log R) is variable. At places where log
653 R was measured directly, it varied between 0.06 and 28.5 mg/cm²/day. The highest
654 precipitation rate was measured at the Terme San Giovanni fissure ridge (28.5 mg/cm²/day)
655 coinciding with the highest positive offset from our empirical calibration curve (Table 1, Figs.
656 6A, 11A). At other places (e.g. Bük, Narrow Gauge springs, Szalajka Creek) precipitation
657 rates are high and Δ_{47} shows also higher values relative to the calibration line (Fig. 6A) but
658 other samples with high precipitation rates (e.g. Tura, Köröm, Igal) plot below the calibration
659 line. Δ_{47} offsets of all travertine and tufa samples calculated relative to water temperature
660 using *eq. 1* show no correlation with precipitation rate (Fig. 8B). Where direct measurements
661 were not possible we qualitatively differentiate sites with low, moderate, high, and very high
662 (cm-to-m/year, comparable to surface corals) deposition. As can be seen in Figure 11B there
663 is no clear correlation between the offset from the calibration regression and the precipitation
664 rates. The morphology of deposited crystals can be affected by their precipitation rate and
665 potentially be used to estimate precipitation rate in case of inactive travertines. However,
666 crystal size can also vary due to several other influencing factors, such as water flow rates or
667 solution chemistry, which can vary through time. To conclude, our data suggest that
668 precipitation rate has no detectable or only minor effects on the Δ_{47} values of these carbonates.

669

670 **Conclusions**

671

672 Recent calcitic and aragonitic travertines and tufa samples precipitating from natural
673 thermal springs and wells, as well as one cave tufa sample, were studied for oxygen and
674 clumped isotopes. Our samples represent a wide temperature and pH range, diverse
675 mineralogy and depositional environments with various precipitation rates from
676 geographically different regions. The majority of our vent and pool travertine data show an
677 oxygen isotope fractionation between the mineral-phase and water compatible with the
678 Tremaine et al. (2011) relationship. No significant difference between the calcite-water and
679 aragonite-water oxygen isotope fractionation could be observed.

680 Δ_{47} data of vent and pool travertines and tufa samples show an excellent correlation
681 with temperature ($r^2 > 0.96$) which is described by the following equation: $\Delta_{47} = (0.044 \pm 0.005$
682 $\times 10^6) / T^2 + (0.205 \pm 0.047)$. The slope of the Δ_{47} -T travertine relationship is intermediate
683 compared to previously published ones, and seems to support the hypothesis that a
684 relationship exists between calibration slopes and acid digestion temperature. The Δ_{47} -T
685 correlation is strong, indicating that factors other than temperature (pH, mineralogy,
686 precipitation rate) have no or only minor effects on the Δ_{47} -signal of carbonates. Our
687 calibration is the most robust available calibration from naturally precipitated inorganic
688 carbonates and it can be used to derive the deposition temperature of ancient carbonate
689 deposits (vent travertine, tufa, cave pool carbonate). Consistent data from three biogenic
690 samples furthermore suggests that the calibration might also be applicable to biogenic
691 carbonates. Using the travertine-based, empirically determined calcite-water oxygen isotope
692 fractionation factor, the $\delta^{18}\text{O}$ values of the travertine and tufa depositing waters can be
693 calculated with more confidence.

694

695 **AUTHOR CONTRIBUTION STATEMENT**

696

697 S. K. and S. M. B. designed the project. S. K. prepared and measured most of the samples at
698 ETH Zürich, interpreted the data and wrote the manuscript. S. M. B., I. M. M., A. N. M., M.
699 Z., S. F. M. B. developed the method at ETH Zürich and wrote parts of the manuscript. I. M.
700 M. prepared and measured some samples. The figures were prepared by S. F. M. B. and S.K..
701 T. K. and C. M. J. provided input to the analysis of the data. E. C., K. H., Z. L., H. Y. and D.
702 J. provided samples for clumped isotope analyses and contributed to the descriptions of the
703 sites. All co-authors contributed to discussions of this work.

704

705 **Acknowledgement**

706

707 The manuscript was improved by helpful comments of Brian Jones, Hagit P. Affek and
708 Aradhna Tripathi. The authors are grateful for XRD analyses by Tibor Németh and for SEM
709 analyses by Gábor Dobosi. The assistance of Stewart Bishop, Madalina Jaggi, Katalin V.
710 Kovács, Andrea Boros and Alexandra Müller in the laboratory work, and Barbara Bódai in
711 the field work are gratefully acknowledged. We thank Norbert Marwan (PIK Potsdam,
712 Germany) for statistical support. S. K. received support by the János Bolyai research
713 scholarship of the Hungarian Academy of Sciences, the Hungarian Scientific Research Fund

714 (OTKA 101664) and the SCIEX postdoctoral Fellowship (ClumpIT; Nr: 13.071-2) at ETH
715 Zürich. Financial support from SNF Project CRSI22_132646/1 STALCLIM to S.F.M.B. and
716 S.B., Swiss NSF projects 200021_143485/1 and 200020-134987 to S.B. and I.M. EU FP7
717 Marie Curie grant No. 298513 to M.Z. and Marie-Heim-Vögtlin grant PMPDP2_139701/1 to
718 A.N.M. are greatly acknowledged. T. K. and J. M. C. gratefully acknowledge funding from
719 the Qatar Carbonates and Carbon Storage Research Centre (QCCSRC), provided jointly by
720 Qatar Petroleum, Shell, and Qatar Science & Technology Park. E. C. is pleased to
721 acknowledge a P.O.R.-F.S.E. 2007-2013 grant from the Tuscan Regional Administration. The
722 authors are grateful to Attila Demény for his financial support of the project. Permission to
723 perform work in Yellowstone National Park was granted to John R. Spear, permit #05664,
724 from the Yellowstone Center for Resources. We are grateful for thoughtful comments of three
725 anonymous reviewers and the associate editor that helped to improve the manuscript.

726

727 **Appendix A. Supplementary material**

728

729 Supplementary material related to this article can be found online at <http://..>

730

731 **References**

732

733 Affek, H. P. (2013) Clumped isotopic equilibrium and the rate of isotope exchange between
734 CO₂ and water. *Am. J. of Sci.* **313**, 309–325.

735

736 Affek, H. P., Bar-Matthews, M., Ayalon, A., Matthews, A., Eiler, J. M. (2008)
737 Glacial/interglacial temperature variations in Soreq cave speleothems as recorded by
738 'clumped isotope' thermometry. *Geochim. Cosmochim. Ac.* **72**, 5351–5360.

739

740 Affek, H. P., Zaarur, S. (2014) Kinetic isotope effect in CO₂ degassing: insight from clumped
741 and oxygen isotopes in laboratory precipitation experiments. *Geochim. Cosmochim. Ac.* **143**,
742 319-330.

743

744 Bárdossy, G., Bottyán, L., Gadó, P., Griger, Á., Sasvári, J. (1980) Automated quantitative
745 phase analysis of bauxites. *American Mineralogist* **65**, 135–141.

746

- 747 Beck, W. C., Grossmann, E. L., Morse, J. W. (2005) Experimental studies of oxygen isotopic
748 fractionation in the carbonic acid system at 15, 25, and 40°C. *Geochim. Cosmochim. Ac.* **69**,
749 3493–3503.
- 750
- 751 Bernasconi S. M., Hu, B., Wacker, U., Fiebig, J., Breitenbach, S. F. M., Rutz, T. (2013)
752 Background effects on Faraday collectors in gas-source mass spectrometry and implications
753 for clumped isotope measurements. *Rapid Comm. Mass Spectrom.* **27**, 603–612.
- 754
- 755 Brogi, A., Liotta, D., Meccheri, M. and Fabbrini, L. (2010) Transtensional shear zones
756 controlling volcanic eruptions: the Middle Pleistocene Mt Amiata volcano (inner Northern
757 Apennines, Italy). *Terra Nova* **22** (2), 137–146.
- 758
- 759 Budd, D. A., Frost, E. L. III, Huntington, K. W., Allwardt, P. F. (2013) Syndepositional
760 deformation features in high/relief carbonate platforms: long-lived conduits for diagenetic
761 fluids. *J. of Sed. Res.* **82**, 12–36.
- 762
- 763 Came, R. E., Eiler, J. M., Veizer, J., Azmy, K., Brand, U., Weidman, C. R. (2007) Coupling
764 of surface temperatures and atmospheric CO₂ concentrations during the Palaeozoic era. *Nature*
765 **449**, 198–202.
- 766
- 767 Came, R. E., Brand, U., Affek, H. P. (2014) Clumped isotope signatures in modern
768 brachiopod carbonate. *Chem. Geol.* **377**, 20–30.
- 769
- 770 Capezzuoli, E., Brogi, A., Ricci, M., Bertini, A. (2011) International School of Travertine &
771 Tufa. *Field Trip Guidebook*. Abbadia San Salvatore 5-9 September 2011, 1–65.
- 772
- 773 Capezzuoli, E., Gandin, A. Sandrelli, F. (2008) Evidence of associated deposition of
774 travertine and calcareous tufa in the Quaternary carbonates of Valdelsa Basin (Tuscany).
775 *Italian J. of Quat. Sci.* **21** (1B), 113–124.
- 776
- 777 Capezzuoli, E., Gandin, A., Pedley, M. (2014) Decoding tufa and travertine (fresh water
778 carbonates) in the sedimentary record: The state of the art. *Sedimentology* **61**, 1–21.
- 779

- 780 Casagli, N., Duchi, V., Pranzini, G. (1990) Low temperature thermal springs of Colle Val
781 d'Elsa (Tuscany, Central Italy). *Memoires of the 22nd Congress of IAH*, XXII, 635–644.
782
- 783 Chafetz, H. S. and Lawrence, J. R. (1994) Stable isotopic variability within modern
784 travertines. *Geogr. Phys. Quat.* **48**, 257–273.
785
- 786 Coplen, T. B. (2007) Calibration of the calcite-water oxygen-isotope geothermometer at
787 Devils Hole, Nevada, a natural laboratory. *Geochim. Cosmochim. Ac.* **71**, 3948–3957.
788
- 789 Daëron, M., Guo, W., Eiler, J., Genty, D., Blamart, D., Boch, R., Drysdale, R. N., Maire, R.,
790 Wainer, K., Zanchetta, G. (2011) ^{13}C - ^{18}O clumping in speleothems: observations from natural
791 caves and precipitation experiments. *Geochim. Cosmochim. Ac.* **75**, 3303–3317.
792
- 793 Day C. C. and Henderson G. M. (2011) Oxygen isotopes in calcite grown under cave-
794 analogue Conditions. *Geochim. Cosmochim. Ac.* **75**, 3956–3972.
795
- 796 Defliese, W.F., Hren, M.T., Lohmann, K.C. (2015) Compositional and Temperature Effects
797 of Phosphoric Acid Fractionation on Δ_{47} Analysis and Implications for Discrepant
798 Calibrations. *Chem. Geol.* **396**, 51-60.
799
- 800 Demény, A., Kele, S., Siklósy, Z. (2010) Empirical equations for the temperature dependence
801 of calcite-water oxygen isotope fractionation from 10 to 70°C. *Rapid Commun. Mass*
802 *Spectrom.* **24**, 3521–3526.
803
- 804 Dennis, K. J. and Schrag, D. P. (2010) Clumped isotope thermometry of carbonatites as an
805 indicator of diagenetic alteration. *Geochim. Cosmochim. Ac.* **74**, 4110–4122.
806
- 807 Dennis, K. J., Affek, H. P., Passey, B. H., Schrag, D. P., Eiler, J. W. (2011) Defining an
808 absolute reference frame for ‘clumped’ isotope studies of CO_2 . *Geochim. Cosmochim. Ac.* **75**,
809 7117–7131.
810
- 811 Di Benedetto, F., Montegrossi, G., Minissale, A., Pardi, L. A., Romanelli, M., Tassi, F.,
812 Delgado Huertas, A., Pampin, E. M., Vaselli, O., Borrini, D. (2011) Biotic and inorganic

- 813 control on travertine deposition at *Bullicame* 3 spring (Viterbo, Italy): A multidisciplinary
814 approach. *Geochim. Cosmochim. Ac.* **75**, 4441–4455.
- 815
- 816 Dietzel, M., Tang, J., Leis, A., Köhler, S. J. (2009) Oxygen isotopic fractionation during
817 inorganic calcite precipitation – Effects of temperature, precipitation rate and pH. *Chem.*
818 *Geol.* **268**, 107–115.
- 819
- 820 Eagle, R. A., Schauble, E. A., Tripathi, A. K., Tutken, T., Hulbert, R. C., Eiler, J. M. (2010)
821 Body temperatures of modern and extinct vertebrates from ^{13}C - ^{18}O bond abundances in
822 bioapatite. *Proc. Natl. Acad. Sci. USA* **107**, 10377–10382.
- 823
- 824 Eagle, R. A., Eiler, J. M., Tripathi, A. K., Ries, J. B., Freitas, P. S., Hiebenthal, C., Wanamaker
825 Jr., A. D., Taviani, M., Elliot, M., Marensi, S., Nakamura, K., Ramirez, P., Roy, K. (2013)
826 The influence of temperature and seawater carbonate saturation state on ^{13}C - ^{18}O bond
827 ordering in bivalve mollusks. *Biogeosci. Disc.* **10**, 157–194
- 828
- 829 Eiler, J. M. (2007) “Clumped-isotope” geochemistry - The study of naturally-occurring,
830 multiply-substituted isotopologues. *Earth Planet. Sci. Lett.* **262**, 309–327.
- 831
- 832 Epstein S., Buchsbaum R., Lowenstam H. and Urey H. C. (1953) Revised carbonate-water
833 isotopic temperature scale. *Bull. Geol. Soc. Am.* **64**, 1315–1326.
- 834
- 835 Epstein, S., Mayeda, T. (1953) Variation of ^{18}O content of waters from natural sources.
836 *Geochim. Cosmochim. Ac.* **4**, 89–103.
- 837
- 838 Fernandez, A. Tang, J., Rosenheim, B. E. (2014) Siderite ‘clumped’ isotope thermometry: A
839 paleoclimate proxy for humid continental environments. *Geochim. Cosmochim. Ac.* **126**, 411–
840 421.
- 841
- 842 Ferry, J. M., Passey, B. H., Vasconcelos, C., Eiler, J. M. (2011) Formation of dolomite at 40-
843 80 °C in the Latemar carbonate buildup, Dolomites, Italy, from clumped isotope thermometry.
844 *Geology* **39**, 571–574
- 845

- 846 Fouke, B. W., Farmer, J. D., Des Marais, D. J., Pratt, L., Sturchio, N. C., Burns, P. C.,
847 Discipulo, M. K. (2000) Depositional facies and aqueous-solid geochemistry of
848 travertinedepositing hot springs (Angel Terrace, Mammoth Hot Springs, Yellowstone
849 National Park, U.S.A.). *J. Sed. Res.* **70**, 565–585.
- 850
- 851 Friedman, I. (1970) Some investigations on the deposition of travertine from Hot Springs-I.
852 The isotopic chemistry of a travertine-depositing spring. *Geochim. Cosmochim. Ac.* **34**, 1303–
853 1315.
- 854
- 855 Gabitov, R. I., Watson, E. B., Sadekov, A. (2012) Oxygen isotope fractionation between
856 calcite and fluid as a function of growth rate and temperature: An in situ study. *Chem. Geol.*
857 **306–307**, 92–102.
- 858
- 859 Ghosh, P., Adkins, J., Affek, H., Balta, B., Guo, W., Schauble, E. A., Schrag, D., Eiler, J. M.
860 (2006a) ^{13}C – ^{18}O bonds in carbonate minerals: A new kind of paleothermometer. *Geochim.*
861 *Cosmochim. Ac.* **70**, 1439–1456.
- 862
- 863 Ghosh, P., Garzzone, C. N., Eiler, J. M. (2006b) Rapid Uplift of the Altiplano Revealed
864 Through ^{13}C – ^{18}O Bonds in Paleosol Carbonates. *Science* **311**, 511–515
- 865
- 866 Ghosh, P., Eiler, J., Campana, S. E., Feeney, R. F. (2007) Calibration of the carbonate
867 ‘clumped isotope’ paleothermometer for otoliths. *Geochim. Cosmochim. Ac.* **71**, 2736–2744.
- 868
- 869 Gonfiantini, R., Panichi, C., Tongiorgi, E. (1968) Isotopic disequilibrium in travertine
870 deposition. *Earth and Planet. Sci. Lett.* **5**, 55–58.
- 871
- 872 Guo, L., Riding, R. (1999) Rapid facies changes in Holocene fissure ridge hot spring
873 travertines, Rapolano Terme, Italy. *Sedimentology* **46**, 1145–1158.
- 874
- 875 Grauel, A.-L. Schmid, T. W., Hu, B., Bergami, C., Capodonti, L., Zhou, L., Bernasconi, S. M.
876 (2013) Calibration and application of the ‘clumped isotope’ thermometer to foraminifera for
877 high-resolution climate reconstructions. *Geochim. Cosmochim. Ac.* **108**, 125–140.
- 878

- 879 Guo, W. (2008) Carbonate clumped isotope thermometry: application to carbonaceous
880 chondrites&effects of kinetic isotope fractionation. *PhD thesis*, California Inst. Techn., 261 p.
881
- 882 Guo W., Mosenfelder, J. L., Goddard III. W. A., Eiler, J. M. (2009) Isotopic fractionations
883 associated with phosphoric acid digestion of carbonate minerals: Insights from first-principles
884 theoretical modelling and clumped isotope measurements. *Geochim. Cosmochim. Ac.* **73**,
885 7203–7225.
886
- 887 Guo, W., Daëron, M., Niles, P., Genty, D, Kim, S. T., Vonhof, H., Affek, H., Wainer, K.,
888 Blamart, D., Eiler, J. (2008) C-13-O-18 bonds in dissolved inorganic carbon: Implications for
889 carbonate clumped isotope thermometry. *Geochim. Cosmochim. Ac.* **72**, A336.
890
- 891 Henkes, G. A., Passey, B. H., Wanamaker Jr., A. D., Grossman, E. L., Ambrose Jr., W. G.,
892 Carroll, M. L. (2013) Carbonate clumped isotope compositions of modern marine mollusk and
893 brachiopod shells. *Geochim. Cosmochim. Ac.* **106**, 307–325.
894
- 895 Hill, P. S., Schauble, E. A., Tripathi, A. K. (2014) Theoretical constraints on the effects of pH,
896 salinity, and temperature on clumped isotope signatures of dissolved inorganic carbon species
897 and precipitating carbonate minerals. *Geochim. Cosmochim. Ac.* **125**, 610–652.
898
- 899 Huntington, K. W., Budd, D. A., Wernicke, B. P., Eiler, J. M. (2011) Use of clumped-isotope
900 thermometry to constrain the crystallization temperature of diagenetic calcite. *J. Sed. Res.* **81**,
901 656–669.
902
- 903 Kármán, K., Maloszewski, P., Deák, J., Fórizs, I., Szabó, Cs. (2014) Transit time
904 determination for a riverbank filtration system using oxygen isotope data and the lumped-
905 parameter model. *Hydrological Sci. J.* **59**, 1109–1116.
906
- 907 Kele, S., Demény, A., Siklósy, Z., Németh, T., Mária, T., Kovács, M. B. (2008) Chemical and
908 stable isotope compositions of recent hot-water travertines and associated thermal waters,
909 from Egerszalók, Hungary: depositional facies and non-equilibrium fractionations. *Sed. Geol.*
910 **211**, 53–72.
911

- 912 Kele, S., Özkul, M., Gökgöz, A., Főrizs, I., Baykara, M.O., Alçiçek, M. C., Németh, T.
913 (2011) Stable isotope geochemical and facies study of Pamukkale travertines: New evidences
914 of low-temperature non-equilibrium calcite-water fractionation. *Sed. Geol.* **238**, 191–212.
915
- 916 Kim, S.-T., O'Neil, J. R. (1997) Equilibrium and nonequilibrium oxygen isotope effects in
917 synthetic carbonates. *Geochim. Cosmochim. Ac.* **61**, 3461–3475.
918
- 919 Kim, S.-T., Hillaire-Marcel, C., Mucci, A. (2006) Mechanisms of equilibrium and kinetic
920 oxygen isotope effects in synthetic aragonite at 25°C. *Geochim. Cosmochim. Ac.* **70**,
921 5790–5801.
922
- 923 Kim, S.-T., Mucci, A., Taylor, B.E. (2007) Phosphoric acid fractionation factors for calcite
924 and aragonite between 25 and 75°C: Revisited. *Chem. Geol.* **246**, 135–146.
925
- 926 Kluge, T., Affek, H. P. (2012) Quantifying kinetic fractionation in Bunker Cave speleothems
927 using Δ_{47} . *Quat. Sci. Rev.* **49**, 82–94.
928
- 929 Kluge, T., Marx, T., Aeschbach-Hertig, W., Riechelmann, S., Riechelmann, D. F. C.,
930 Wackerbarth, A., Fohlmesiter, J., Scholz, D., Mangini, A., Immenhauser, A., Richter, D. K.,
931 Spötl, C., Affek, H. P. (2013) Reconstruction of drip-water $\delta^{18}\text{O}$ based on calcite oxygen and
932 clumped isotopes of speleothems from Bunker Cave (Germany). *Climate of the Past* **9**,
933 377–391.
934
- 935 Kluge, T., Affek, H. P., Zhang, Y.G., Dublyansky, Y., Spötl, C., Immenhauser, A., Richter,
936 D.K. (2014a) Clumped isotope thermometry of cryogenic cave carbonates.
937 *Geochim. Cosmochim. Ac.* **126**, 541–554.
938
- 939 Kluge, T., Affek, H. P., Dublyansky, Y., Spötl, C. (2014b) Devils Hole paleotemperatures and
940 implications for oxygen isotope equilibrium fractionation. *Earth and Plan. Sci. Lett.* **400**,
941 251–260.
942
- 943 Kluge, T., John, C.M. (2015) Effects of brine chemistry and polymorphism on clumped
944 isotopes revealed by laboratory precipitation of mono- and multiphase calcium carbonates,
945 *Geochim. Cosmochim. Ac.* **160**, 155–168.

- 946
947 Kluge, T., John, C.M., Jourdan, A.-L., Davis, S., Crawshaw, J. (2015) Laboratory calibration
948 of the calcium carbonate clumped isotope thermometer in the 25-250°C temperature range
949 *Geochim. Cosmochim. Ac.* **157**, 213-227.
950
- 951 Liu, Z., Sun, H., Lu, B., Liu, X., Ye, W. and Zeng, C. (2010) Wet-dry seasonal variations of
952 hydrochemistry and carbonate precipitation rates in a travertine-depositing canal at Baishuitai
953 Yunnan, SW China: implications for the formation of biannual laminae in travertine and for
954 climatic reconstruction. *Chem.Geol.* **273**, 258–266.
955
- 956 McCrea, J. M. (1950) On the isotopic chemistry of carbonates and a paleotemperature scale.
957 *J. of Chem. Phys.* **18**, 849–857.
958
- 959 Meckler, A. N., Ziegler, M., Millan, I. M., Breitenbach, S. F. M., Bernasconi, S. M. (2014)
960 Long-term performance of the Kiel carbonate device with a new correction scheme for
961 clumped isotope measurements. *Rapid Commun. Mass Spec.* **28**, 1705–1715.
962
- 963 Minissale, A. (2004) Origin, transport and discharge of CO₂ in central Italy. *Earth-Sci. Rev.*
964 **66**, 89–141.
965
- 966 Passey, B. H., Levin, N. E., Cerling, T. E., Brown, F. H. , Eiler, J. M. (2010) High-
967 temperature environments of human evolution in East Africa based on bond ordering in
968 paleosol carbonates. *Proceedings of the National Academy of Sciences of the United States of*
969 *America* **2010**, *107*, 11245.
970
- 971 Pentecost, A. (1995) Geochemistry of carbon dioxide in six travertine-depositing waters of
972 Italy. *J. Hydr.* **167**, 263–278.
973
- 974 Petrizzo, D.A., Young, E.D., Runnegar, B.N. (2014) Implications of high-precision
975 measurements of ¹³C–¹⁸O bond ordering in CO₂ for thermometry in modern bivalve mollusc
976 shells. *Geochim. Cosmochim. Ac.* **142**, 400–410.
977
- 978 Sachs, L. (1984) Applied statistics: a handbook of techniques. Springer-Verlag. 707 pp.
979

- 980 Saenger, C., Affek, H. P., Felis, T., Thiagarajan, N., Lough, J. M., Holcomb, M. (2012)
981 Carbonate clumped isotope variability in shallow water corals: Temperature dependence and
982 growth-related vital effects. *Geochim. Cosmochim. Ac.* **99**, 224–242.
- 983
- 984 Schauble, E. A., Ghosh, P., Eiler, J. (2006) Preferential formation of ^{13}C – ^{18}O bonds in
985 carbonate minerals, estimated using first principle lattice dynamics. *Geochim. Cosmochim.*
986 *Ac.* **70**, 2510–2529.
- 987
- 988 Schmid, T. W., Bernasconi, S. M. (2010) An automated method for ‘clumped isotope’
989 measurements on small carbonate samples. *Rapid Commun. Mass Spec.* **24**, 1955–1963.
- 990
- 991 Snell, K. E., Thrasher, B. L., Eiler, J. M., Koch, P. L., Sloan, L. C., Tabor, N. J. (2013) Hot
992 summers in the Bighorn Basin during the early Paleogene greenhouse. *Geology* **41**, 95–96.
- 993
- 994 Tang, J., Dietzel, M., Fernandez, A., Tripathi, A. K., Rosenheim, B. E. (2014) Evaluation of
995 kinetic effects on clumped isotope fractionation (Δ_{47}) during inorganic calcite precipitation.
996 *Geochim. Cosmochim. Ac.* **134**, 120–136
- 997
- 998 Thiagarajan, N., Adkins, J., Eiler, J. (2011) Carbonate clumped isotope thermometry of deep-
999 sea corals and implications for vital effects. *Geochim. Cosmochim. Ac.* **75**, 4416–4425.
- 1000
- 1001 Tremaine, D.M., Froelich, P.N., Wang, Y. (2011) Speleothem calcite farmed in situ: Modern
1002 calibration of $\delta^{18}\text{O}$ and $\delta^{13}\text{C}$ paleoclimate proxies in a continuously-monitored natural cave
1003 system. *Geochim. Cosmochim. Ac.*, **75**, 4929–4950.
- 1004
- 1005 Tripathi, K. A., Eagle, R. A., Thiagarajan, N., Gagnon, A. C., Bauch, H., Halloran, P. R., Eiler,
1006 J. M. (2010) ^{13}C – ^{18}O isotope signatures and ‘clumped isotope’ thermometry in foraminifera
1007 and coccoliths. *Geochim. Cosmochim. Ac.* **74**, 5697–5717.
- 1008
- 1009 Tripathi, A. K. and Hill, P. S. (2014) In search of processes driving clumped-isotope
1010 (dis)equilibrium. California, Goldschmidt 2014 abstracts, 2520
- 1011
- 1012 Turi, B. (1986) Stable isotope geochemistry of travertines: In: Fritz, B.P., Fontes, J.C. (Eds.),
1013 *Handbook of Environmental Isotope Geochemistry*. Elsevier, Amsterdam.

- 1014
- 1015 Usdowski, E., Michaelis, J., Böttcher, M. E., Hoefs, J. (1991) Factors for the oxygen isotope
1016 equilibrium fractionation between aqueous and gaseous CO₂, carbonic acid, bicarbonate,
1017 carbonate, and water (19°C). *Z. Phys. Chem.* **170**, 237–249.
- 1018
- 1019 Wacker, U., Fiebig, J., and Schöne, B.R. (2013) Clumped isotope analysis of carbonates:
1020 comparison of two different acid digestion techniques. *Rapid Commun. Mass Spectrom.* **27**,
1021 1631-1642.
- 1022
- 1023 Wacker, U., Fiebig, J., Tödter, J., Schöne, B. R., Bahr, A., Friedrich, O., Tütken, T., Gischler,
1024 E., Joachimski, M. M. (2014) Empirical calibration of the clumped isotope paleothermometer
1025 using calcites of various origins. *Geochim. Cosmochim. Ac.* **141**, 127–144.
- 1026
- 1027 Wainer, K., Genty, D., Blamart, D., Daëron, M., Bar-Matthews, M., Vonhof, H., Dublyansky,
1028 Y., Pons-Branchu, E., Thomas, L., van Calsteren, P., Quinif, Y., Caillon, N. (2011)
1029 Speleothem record of the last 180 ka in Villars cave (SW France): investigation of a large
1030 $\delta^{18}\text{O}$ shift between MIS6 and MIS5. *Quat. Sci. Rev.* **30**, 130–146.
- 1031
- 1032 Wang, H., Yan, H., Liu, Z. (2014) Contrasts in variations of the carbon and oxygen isotopic
1033 composition of travertines formed in pools and a ramp stream at Huanglong Ravine, China:
1034 Implications for paleoclimatic interpretations. *Geochim. Cosmochim. Ac.* **125**, 34–48
- 1035
- 1036 Yan, H., Sun, H., Liu, Z. (2012) Equilibrium vs. Kinetic fractionation of oxygen isotopes in
1037 two low-temperature travertine-depositing systems with differing hydrodynamic conditions at
1038 Baishuitai, Yunnan, SW China. *Geochim. Cosmochim. Ac.* **95**, 63–78.
- 1039
- 1040 Zaarur, S., Olcak, G., Affek, H. P. (2011) Paleo-environmental implication of clumped
1041 isotopes in land snail shells. *Geochim. Cosmochim. Ac.* **75**, 6859–6869.
- 1042
- 1043 Zaarur, S., Affek, H. P., Brandon, M. (2013) A revised calibration of the clumped isotope
1044 thermometer. *Earth Planet Sci. Lett.* **382**, 47–57.
- 1045
- 1046 Zeebe R. E. (1999) An explanation of the effect of seawater carbonate concentration on
1047 foraminiferal oxygen isotopes. *Geochim. Cosmochim. Ac.* **63**, 2001–2007.

1048

1049 Zeebe, R. E. (2007) An expression for the overall oxygen isotope fractionation between the
1050 sum of dissolved inorganic carbon and water. *Geochem. Geophys. Geos.* **8** (9), Q09002.
1051 doi:10.1029/2007GC001663.

ACCEPTED MANUSCRIPT

Figure and table captions**Fig. 1**

Field photos of the travertine sites with the sampling points:

- A) Recent travertine deposits and thermal pool of Palagio.
- B) Sampling point at Bagnoli thermal spring (precipitation at the tube outlet).
- C) Reddish–brownish recent travertine at the discharge point of the Acqua Borra spring.
- D) Recently active part of the Terme San Giovanni fissure–ridge.
- E) Tap of the Madonna al Colle Well drilled for geothermal exploration.
- F) Small and actively forming travertine mounds indicate the discharge points of the Il Doccio spring located on the riverbank.
- G) Opened thermal spa with recent travertine deposition directly on the riverbank at Bagni di Petriolo.
- H) The outlet of the Fosso Bianco spring (Bagni San Filippo).

Fig. 2

Travertine sites with the sampling points:

- A) Vent pool at Piscine Carletti (Viterbo, Italy).
- B) Carbonate deposits in the cellar of the Széchenyi thermal spa.
- C) The Bük thermal well with its recent carbonate deposit.
- D) Carbonate encrustation within the tube of the Igal thermal well.
- E) Recent aragonitic travertine deposition at the Köröm thermal well.
- F) Terraced slope travertine deposit (P5) at Baishuitai (China).
- G) Vent pool outlet (sample NG-2) at Narrow Gauge Springs (Mammoth Hot Springs, Yellowstone, USA).

Fig. 3

Tufa deposits from karstic creeks and caves. The scale bars represents 20 cm.

- A-C) Calcareous tufa encrustations and dams (samples Szal-2, Szal-6, Szal-15) in Szalajka Creek (Hungary).
- D) Creek bed tufa encrustation at Sarteano (Italy) and at Canatoppa (E).
- F) Perched spring tufa deposit at La Pigna (Italy).
- G) Recent, periodically forming tufa deposit (Havasok tufa) from Baradla cave (Hungary).

Fig. 4

SEM photomicrographs of some selected travertine samples (**Table 1**) showing the variety of crystal shapes and sizes:

- A) Calcite crystals and extracellular polymeric substances (EPS) produced by microorganisms (Bagni San Filippo, Fosso Bianco).
- B) Dendritic structures resembling calcite "feather-like" crystals (Il Doccio).
- C) Gypsum crystals within the calcite (Bagni di Petriolo).
- D) Calcite and goethite (Acqua Borra).
- E) Diatoms within the calcitic-aragonitic travertine (well deposit) of Rapolano Terme.

- 52 F) Dendritic calcite with gypsum crystal (Terme San Giovanni).
 53 G) EPS filaments and diatom like structures within calcite (Bagnoli).
 54 H) EPS filaments within aragonitic travertine of Palagio.

55
 56 **Fig. 5**

57
 58 A) Observed $1000\ln\alpha_{\text{CaCO}_3\text{-water}}$ values versus precipitation temperatures. The Devils Hole data
 59 point from Coplen (2007) is plotted for comparison. B) Same as A, but coded according to
 60 mineralogy. The error bars for $1000\ln\alpha_{\text{CaCO}_3\text{-water}}$ values are smaller than the size of the
 61 symbols.

62
 63 **Fig. 6**

64
 65 A) Correlation between precipitation temperature and Δ_{47} of all analyzed recent travertine,
 66 tufa and cave carbonates and three biogenic samples. The empirical Δ_{47} - T calibration is
 67 based on vent and pool travertine samples. Tufa samples are also shown, together with the Δ_{47}
 68 value of recent calcite raft and vein calcite sample from Devils Hole (Kluge et al., 2014b).

69
 70 B) Δ_{47} values of vent and pool samples with different calcite/aragonite ratio versus
 71 temperature.

72
 73 **Fig. 7**

74
 75 Comparison of the $1000\ln\alpha_{\text{CaCO}_3\text{-water}}$ values determined in this study with those from Kim and
 76 O'Neil (1997), Affek and Zaarur (2014), Coplen (2007) based on Devils Hole calcite and the
 77 cave-specific calibration line of Tremaine et al. (2011).

78
 79 **Fig. 8**

80
 81 Comparison of the temperature dependence of Δ_{47} of travertines with other published studies.
 82 Note the steeper slopes obtained with acid reaction temperature of 25°C (Zaarur et al., 2013),
 83 and the lower slope for carbonates reacted at 90°C (Wacker et al., 2014). For comparison we
 84 also show the theoretical relationship of Guo et al. (2009) and the surface precipitates from
 85 Affek and Zaarur (2014).

86
 87 **Fig. 9**

88
 89 A) Observed $1000\ln\alpha$ values versus Δ_{47} values.

90
 91 B) Offsets in Δ_{47} versus offsets in $1000\ln\alpha_{\text{CaCO}_3\text{-water}}$ from the respective calibration lines
 92 determined in this study do not show any significant correlation. The error bar represents the
 93 average analytical error in Δ_{47} , the analytical error in $1000\ln\alpha$ is smaller than the size of the
 94 symbols.

95
 96 **Fig. 10**

97
 98 A) Temperature dependence of Δ_{47} of travertines and tufa grouped according to pH. B) Δ_{47}
 99 offsets from the calibration line (eq. 1) versus pH. The error bar represents the average
 100 analytical error in Δ_{47} .

101
 102 **Fig. 11**

103
104 A) Temperature dependence of Δ_{47} of travertines and tufa grouped by precipitation rate.

105
106 B) Δ_{47} offsets from the calibration line (*eq. 1*) versus precipitation rate (arbitrary scale). The
107 error bar represents the average analytical error in Δ_{47} .

108
109 **Table 1**

110
111 Mineralogy, facies types, physico-chemical parameters T, pH and EC, TDS, precipitation
112 rate, crystal size and isotopic composition ($\delta^{13}\text{C}_{\text{travertine}}$, $\delta^{18}\text{O}_{\text{travertine}}$, δ^{47} , Δ_{47} , $\delta^{18}\text{O}_{\text{water}}$) of the
113 studied samples. Δ_{47} data are reported in the absolute reference frame. "N" is the number of
114 analyzed aliquots of the sample. The Δ_{47} offset is calculated with regard to Δ_{47} obtained using
115 *eq. 1*. T_{expected} shows temperatures calculated using measured Δ_{47} data and *eq. 1*. The $1000\ln\alpha$
116 offset refers to the difference between the observed calcite-water oxygen isotope fractionation
117 factor and the fractionation factors calculated using the travertine equation of this study. T
118 and pH values of the Madre del Agua sample are from Demény et al. (2010). Data of the
119 Baishuitai travertine samples are taken from Yan et al. (2012). $\delta^{18}\text{O}$ values of three aragonitic
120 travertines (Köröm, Széchenyi thermal spa, Palagio) were corrected by -0.42% , according to
121 the aragonite acid digestion fractionation factor of Kim et al. (2007).

122

123 **Table 2**

124
125 Mineralogy and isotopic composition ($\delta^{13}\text{C}$, $\delta^{18}\text{O}$, δ^{47} , Δ_{47}) of the biogenic samples. Δ_{47} data
126 are reported in the absolute reference frame. "N" is the number of analyzed aliquots for each
127 sample.

128

129

Table 1

| Site name | GPS coordinates (degree, min, sec) | Sample name | material | mineralogy (%) | origin | facies | T (°C) | pH | EC (mS/cm) | log R (mg/cm ² /d) | crystal size and shape (µm) |
|------------------------------------|---------------------------------------|-----------------|------------|----------------------------|------------------|--------------------------------------|-----------|------|---------------|----------------------------------|----------------------------------|
| Tura | N47°36'36", E19°34'17" | Tu-4 well/2000 | travertine | 97 % cc, 3% ar | thermal well | vent | 95.0 | 6.88 | 3.04 | intensive | |
| Igal | N46°32'37", E17°56'42" | B-1/2011 | travertine | 100 % cc | thermal well | vent (tube encrustation) | 75.0 | 6.89 | 12.24 | intensive | |
| Bük | N47°22'25", E16°46'35" | Bük-4 | travertine | 98 % cc, 1% ar | thermal well | vent (tube outlet) | 54.9 | 6.88 | 12.90 | intensive | |
| Szèchenyi Spa, Budapest* | N47°31'07", E19°05'03" | SZ-2/2 | travertine | 20% cc, 80 % ar | thermal well | tube encrustation | 70.9 | 6.40 | 1.57 | intensive | |
| Köröm* | N47°59'49", E20°59'14" | Kör 13/0 | travertine | 97 % ar., 3 % cc | thermal well | vent | 79.2 | 6.80 | 1.38 | intensive | |
| Madre del Agua, Tenerife | N28°10'57", W16°35'40" | Canarian | travertine | 100 % cc | natural spring | channel discharge | 33.8 | 7.70 | n.d. | moderate | |
| Acqua Borra | N43°18'28", E11°25'41" | Acqua Borra | travertine | 85% cc, 15% goethite | natural spring | tube outlet | 36.1 | 6.58 | > 20 | 2.14 (moderate) | no crystal shape |
| Bagni di Petriolo | N43°04'45", E11°17'32" | BP | travertine | 75% cc, 12% gypsum, 10% S | natural spring | tube outlet | 44.3 | 6.45 | 4.54 | moderate | 70 (rhomb.), gypsum (100-200), |
| Bagnoli | N43°26'39", E11°03'15" | Bagnoli | travertine | 95% cc, 2% gypsum, 3% Q | natural spring | tube outlet | 23.7 | 6.62 | 2.98 | 0.06 (very low) | 30-50 (rhomb.), microbial mats |
| Bagni San Filippo, Fosso Bianco | N42°55'39", E11°42'10" | BSF- FB | travertine | 99% cc, 1%>ar, 1%>gypsum | natural spring | spring outlet | 44.6 | 6.53 | 3.54 | 1 (moderate) | 50 (dendritic) |
| Il Doccio | N43° 09'27", E11°17'08" | Il Doccio | travertine | 60% cc, 35% gypsum, 3-5% S | natural spring | vent | 48.3 | 7.05 | 8.7 | 0.1 (low) | 50-70 (dendritic) |
| Palagio* | N43°29'51", E10°52'18" | Palagio | travertine | 99% ar, 1% Q | natural spring | pool (raft) | 22.7 | 6.57 | 6.36 | 0.61 (moderate) | no crystal shape, microbial mats |
| Rapolano Terme | N43°17'58", E11°36'11" | R T-1 | travertine | 80% cc, 20% ar | thermal well | water leak of a thermal well | 28 | 6.62 | 5.72 | low | 50 (rhomb.), diatoms (10) |
| Terme San Giovanni | N43°16'43", E11°35'34" | TSG | travertine | 90% cc, 2 % ar, 8% gypsum | natural spring | small pool on a fissure ridge (raft) | 41.2 | 6.53 | 6.29 | 28.5 (very intensive) | 20-50 (dendritic), gypsum (100) |
| Piscine Carletti, Viterbo | N42°25'18", E12°03'53" | P. Carletti-8.1 | travertine | 98% cc, 1%> ar. | natural spring | closest to vent channel sample | 57.9 | 5.67 | 2.95 | low | |
| Baishuitai | N27°30', E100°02' | P5 summer | travertine | 100 % cc | natural spring | pool | 12.0 | 8.14 | 0.76 | 0.66 (moderate) | |
| Baishuitai | N27°30', E100°02' | P5 winter | travertine | 100 % cc | natural spring | pool | 5.6 | 8.19 | 0.802 | 0.44 (moderate) | |
| Narrow Gauge (M.H.S., Yellowstone) | N44°34'52", W110°25'24" | NG-2 | travertine | 95 % cc, 5% ar, S | natural spring | vent pool outlet | 60.4 | 6.6 | 1.38 | intensive | |
| Sarteano | N42°59'52", E11°53'00" | SAR | tufa | 100 % cc | karstic spring | downstream (100 m) | 20.7 | 8.92 | 2.11 | moderate | |
| Canatoppa | N43°16'41", E11°35'20" | CAN | tufa | 100 % cc | karstic spring | downstream sample | 11 | 8.94 | 1.65 | moderate | |
| La Pigna | N43°06'38", E11°15'43" | LAP | tufa | 100 % cc | karstic spring | downstream (20 m, below a cascade) | 12.5 | 8.61 | 0.55 | moderate | |
| Szalajka | N48°05'27", E20°24'09" | Szal-2 | tufa | 95 %cc, 5 % detrital min. | karstic spring | downstream tufa dam | 10.1 | 8.45 | 0.503 | intensive | |
| Szalajka | N48°05'27", E20°24'09" | Szal-6 | tufa | 96 %cc, 5 % detrital min. | karstic spring | downstream tufa dam | 11.0 | 8.55 | 0.473 | intensive | |
| Szalajka | N48°05'27", E20°24'09" | Szal-15 | tufa | 97 %cc, 5 % detrital min. | karstic spring | downstream tufa dam | 12.1 | 8.53 | 0.484 | intensive | |
| Havasok | N48°28'17", E20°29'44" | Havasok | cave tufa | 100 % cc | cave karst water | cascade/pool rim | 9.5 | n.d. | n.d. | very low | |

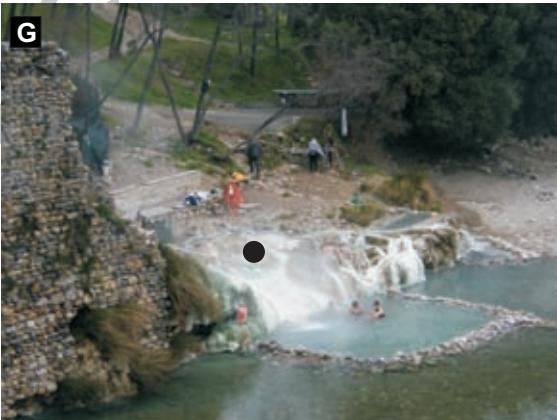
Table 1 contd.

| Site name | $\delta^{13}\text{C}_{\text{trav}}$ (‰, PDB) | $\delta^{18}\text{O}_{\text{trav}}$ (‰, SMOW) | $\delta^{18}\text{O}_w$ (‰ SMOW) | δ^{47} (‰) | Δ_{47} (‰) | S.E. ± | N | Δ_{47} calculated (using eq.1 ; ‰) | Δ_{47} offset (from eq.1 ; ‰) | T_{expected} (using eq.1) | 1000 ln α obs. (‰) | 1000 ln α calculated (using empirical eq ; ‰) | 1000 ln α offset (from emp. eq ; ‰) |
|------------------------------------|---|--|-------------------------------------|----------------------|----------------------|-----------|------|--|---|---------------------------------------|------------------------------|---|---|
| Tura | 3.78 | 6.89 | -12.4 | -6.648 | 0.51 | 0.012 | 30 | 0.525 | -0.015 | 104 | 19.3 | 18.33 | 1.02 |
| Igal | 0.75 | 16.84 | -4.0 | 0.474 | 0.555 | 0.013 | 30 | 0.563 | -0.008 | 79 | 20.7 | 21.45 | -0.74 |
| Bük | 2.34 | 15.27 | -9.9 | 0.507 | 0.625 | 0.016 | 27 | 0.609 | 0.016 | 49 | 25.1 | 24.97 | 0.14 |
| Szèchenyi Spa, Budapest* | 2.9 | 9.33 | -12.6 | -4.562 | 0.567 | 0.011 | 30 | 0.572 | -0.005 | 73 | 22.0 | 22.13 | -0.16 |
| Köröm* | 3.62 | 7.84 | -11.5 | -5.399 | 0.545 | 0.004 | 37 | 0.554 | -0.009 | 84 | 19.4 | 20.76 | -1.39 |
| Madre del Agua, Tenerife | 0.24 | 20.14 | -8.1 | 3.384 | 0.656 | 0.012 | 29 | 0.667 | -0.011 | 37 | 28.1 | 29.16 | -1.09 |
| Acqua Borra | 2.99 | 22.98 | -5.2 | 8.884 | 0.655 | 0.025 | 30 | 0.660 | -0.005 | 38 | 27.9 | 28.67 | -0.74 |
| Bagni di Petriolo | 3.3 | 21.23 | -6.4 | n.d. | n.d. | n.d. | n.d. | n.d. | | n.d. | 27.4 | 27.00 | 0.43 |
| Bagnoli | 5.64 | 25.36 | -7.0 | 13.859 | 0.695 | 0.010 | 22 | 0.699 | -0.004 | 25 | 32.1 | 31.37 | 0.70 |
| Bagni San Filippo, Fosso Bianco | 7.45 | 20.74 | -7.9 | 10.931 | 0.644 | 0.004 | 30 | 0.636 | 0.008 | 42 | 28.5 | 26.94 | 1.52 |
| Il Doccio | 2.4 | 19.99 | -5.9 | n.d. | n.d. | n.d. | n.d. | 0.626 | | n.d. | 25.7 | 26.22 | -0.51 |
| Palagio* | 2.47 | 24.63 | -7.0 | 10.09 | 0.696 | 0.018 | 30 | 0.703 | -0.007 | 25 | 31.4 | 31.60 | -0.24 |
| Rapolano Terme | 3.8 | 23.15 | -6.9 | 9.851 | 0.68 | 0.016 | 33 | 0.685 | -0.005 | 30 | 29.8 | 30.41 | -0.61 |
| Terme San Giovanni | 2.58 | 21.73 | -6.9 | 7.254 | 0.678 | 0.012 | 28 | 0.645 | 0.033 | 30 | 28.4 | 27.62 | 0.80 |
| Piscine Carletti, Viterbo | 7.25 | 18.18 | -6.5 | 8.109 | 0.603 | 0.007 | 30 | 0.601 | 0.002 | 57 | 24.5 | 24.41 | 0.12 |
| Baishuitai | 5.63 | 16.14 | n.d. | 4.615 | 0.741 | 0.013 | 37 | 0.741 | 0.000 | 12 | n.d. | 34.14 | n.d. |
| Baishuitai | 5.28 | 17.66 | n.d. | 5.809 | 0.749 | 0.013 | 38 | 0.766 | -0.017 | 10 | n.d. | 35.75 | n.d. |
| Narrow Gauge (M.H.S., Yellowstone) | 3.98 | 5.65 | -17.9 | -7.658 | 0.601 | 0.009 | 29 | 0.595 | 0.006 | 58 | 23.7 | 23.96 | -0.27 |
| Sarteano | 0.55 | 23.3 | -7.8 | 6.844 | 0.703 | 0.009 | 29 | 0.710 | -0.007 | 23 | 30.8 | 32.06 | -1.22 |
| Canatoppa | -3.97 | 25.32 | -6.5 | 4.517 | 0.742 | 0.008 | 29 | 0.745 | -0.003 | 12 | 31.6 | 34.39 | -2.82 |
| La Pigna | -11.27 | 25.08 | -6.8 | -2.806 | 0.73 | 0.021 | 31 | 0.739 | -0.009 | 15 | 31.6 | 34.02 | -2.43 |
| Szalajka | -10.2 | 22.19 | -10.6 | -4.616 | 0.755 | 0.006 | 27 | 0.748 | 0.007 | 8 | 32.6 | 34.61 | -2.01 |
| Szalajka | -9.86 | 21.94 | -10.6 | -4.553 | 0.732 | 0.008 | 29 | 0.745 | -0.013 | 14 | 32.4 | 34.39 | -2.03 |
| Szalajka | -9.44 | 21.33 | -10.7 | -4.719 | 0.76 | 0.008 | 23 | 0.741 | 0.019 | 7 | 31.9 | 34.11 | -2.25 |
| Havasok | -10.95 | 22.95 | -9.7 | -4.586 | 0.756 | 0.01 | 30 | 0.751 | 0.005 | 8 | 32.4 | 34.76 | -2.32 |

Table 2

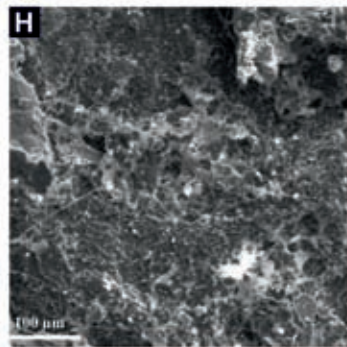
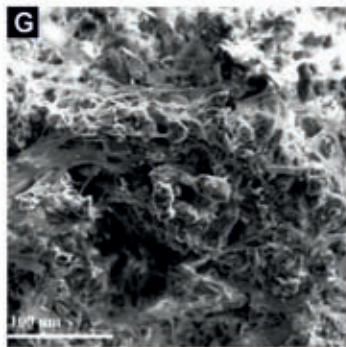
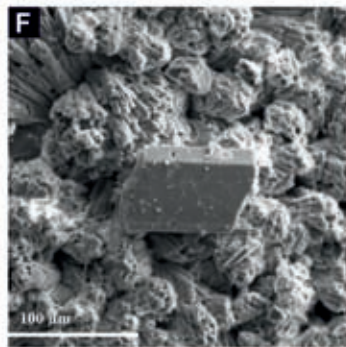
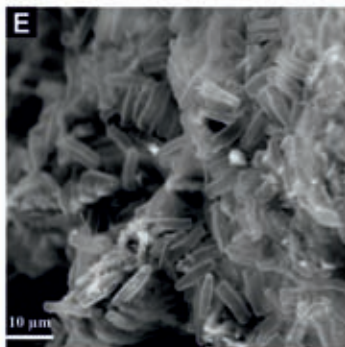
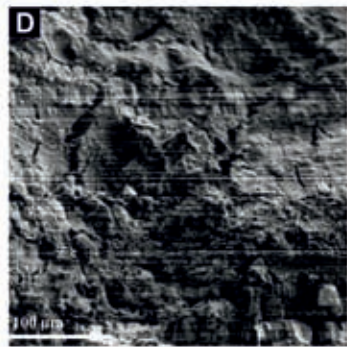
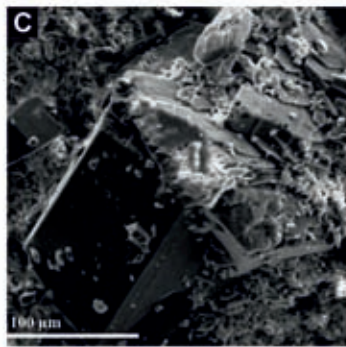
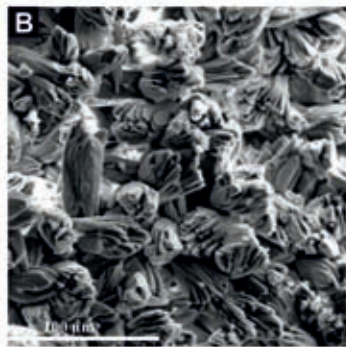
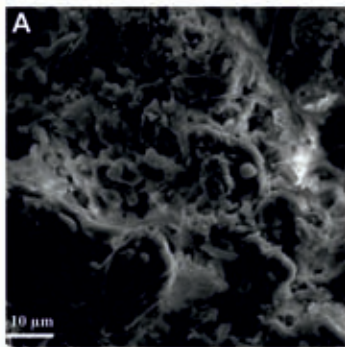
| Sample name | material | mineralogy | T (°C) | $\delta^{13}\text{C}$ (‰, PDB) | $\delta^{18}\text{O}_{\text{cc}}$ (‰, PDB) | δ^{47} (‰) | Δ_{47} (weighted average) (‰) | SE ± | N |
|--------------------------|------------|------------|-----------|-----------------------------------|---|----------------------|---|--------------|----|
| <i>Arctica Islandica</i> | bivalve | aragonite | 6 | 1.67 | 3.48 | 19.30 | 0.759 | 0.004 | 40 |
| <i>Dyscolia wyvillei</i> | brachiopod | calcite | 10 | 2.51 | 2.47 | 19.06 | 0.742 | 0.018 | 36 |
| Eggshell of an Ostrich | eggshell | calcite | 38 | -12.68 | -3.84 | -2.34 | 0.648 | 0.014 | 36 |

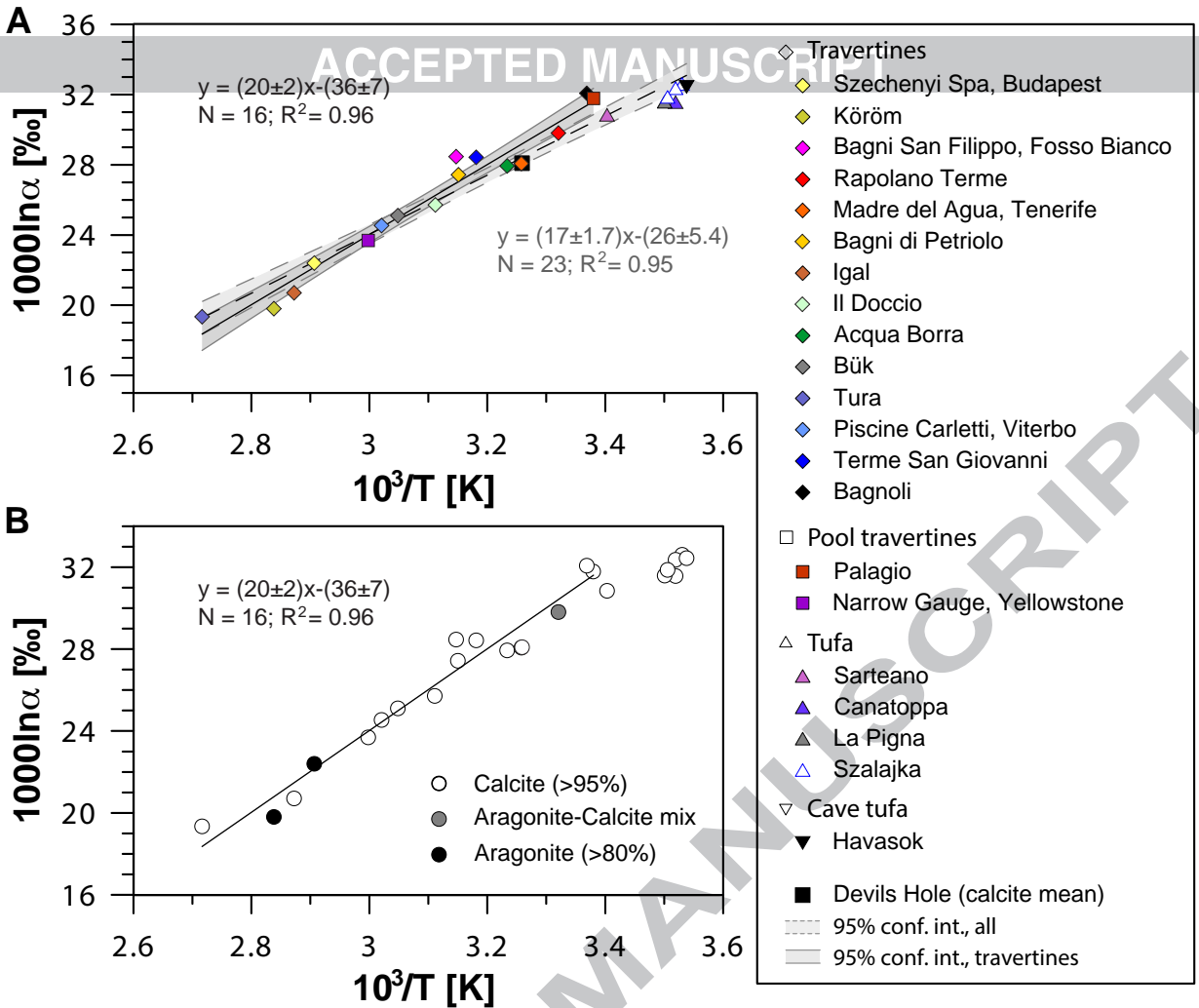
ACCEPTED MANUSCRIPT

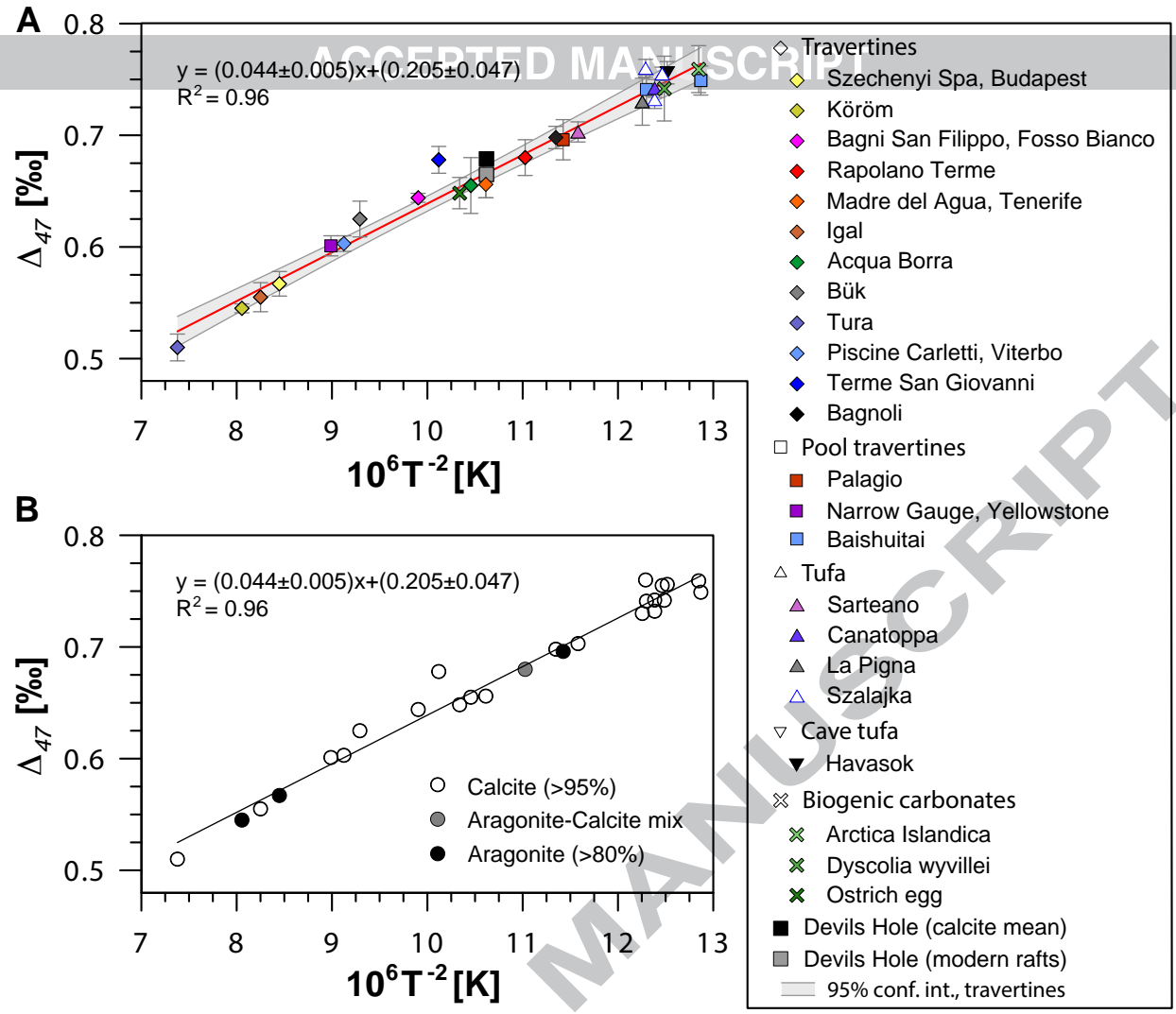


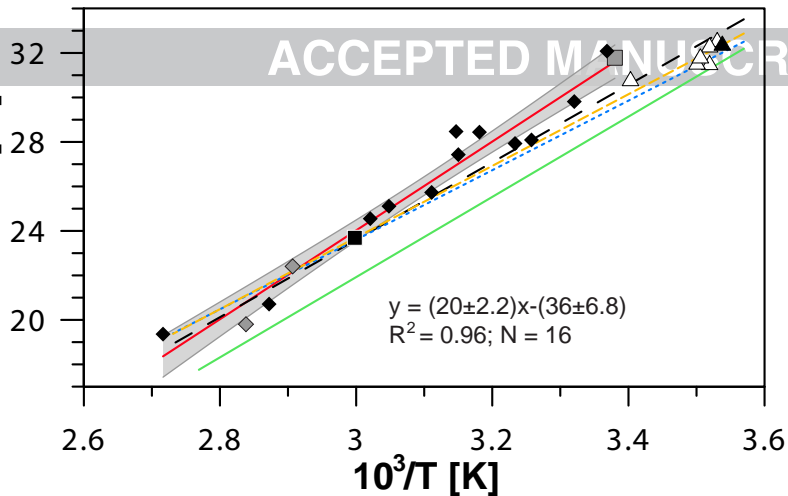










$1000\ln\alpha$ [‰]

- Kim & O'Neil (1997)
- - Coplen (2007)
- - Tremaine et al. (2011)
- ⋯ Affek & Zaarur (2014)
- ◆ Vent calcite
- ◇ Vent aragonite
- Pool calcite
- Pool aragonite
- △ Tufa calcite
- ▲ Cave calcite
- 95% conf. int. (travertines)

